UCRL-ID-123468

Mechanical Characterization of Sonar Window Materials

S. J. DeTeresa
S. E. Groves
P. J. Harwood
R. J. Sanchez

March 25, 1996

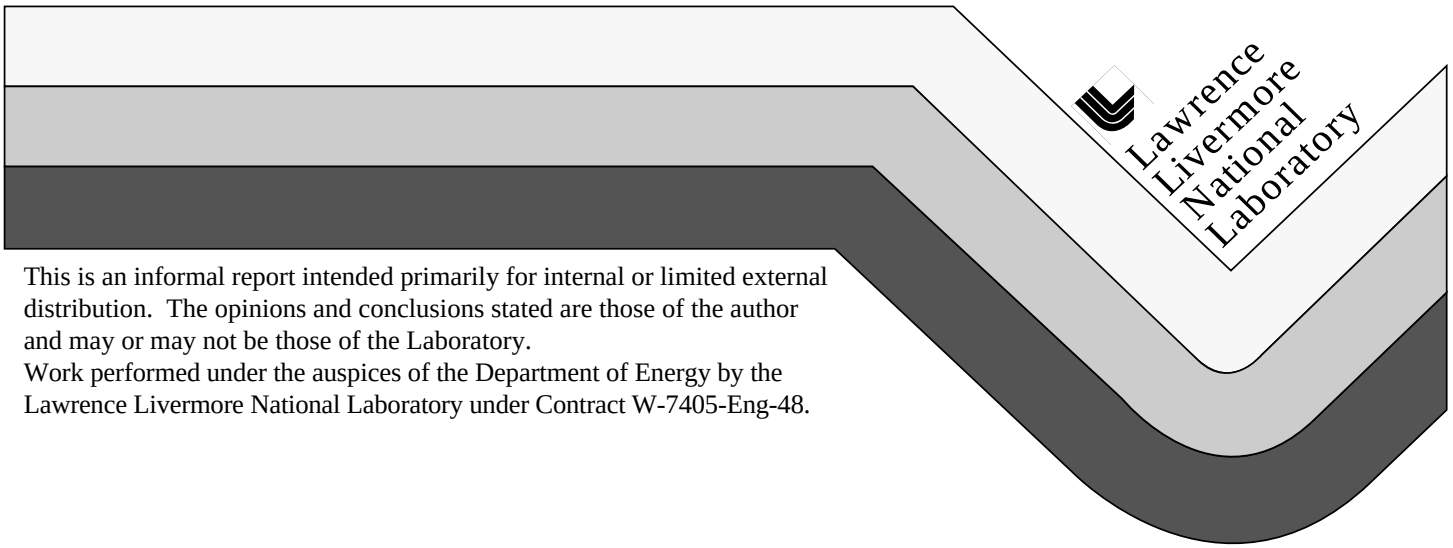

Work performed under the auspices of the Department of Energy by the Lawrence Livermore National Laboratory under Contract W-7405-Eng-48.

Sonar Window Materials Characterization

for

The Office of Naval Research

and

The Naval Undersea Warfare Center, New London

Final Report

Mechanical Characterization of Sonar Window Materials

S. J. DeTeresa, S. E. Groves, P. J. Harwood and R. J. Sanchez
Polymer Composites Group
Manufacturing and Materials Engineering Division
Lawrence Livermore National Laboratory
Livermore, California

25 March, 1996

Abstract

The three-dimensional mechanical behavior of thick Spectra/epoxy sonar window materials containing various special material layers is summarized in this report. Three different materials, which were fabricated by two companies known as "A" and "B," were received from the Naval Undersea Warfare Center (NUWC), New London, Connecticut. The three materials designated: "A with microspheres (Aμ)," "A without microspheres (A)," and "B" were measured for all properties. The total number of tests was reduced through the assumption that the two orthogonal, in-plane directions were identical. Consequently, these materials should have only six independent elastic constants. The measured constants and one redundant value are summarized in Table 1 and the strengths are given in Table 2.

Table 1. Summary of elastic constants.

	Material		
Property	**Aμ**	**A**	**B**
$E_{11}=E_{22}$ (Msi)			
Tension	2.0	2.9	1.9
Compression	2.6	4.0	3.3
ν_{12}			
Tension	0.15	0.06	0.06
Compression	0.20	0.10	0.10
$\nu_{13}=\nu_{23}$			
Tension	0.54	0.35	0.65
Compression	0.38	0.55	0.63
E_{33} (ksi)			
Compression	100	190	660
$\nu_{31}=\nu_{32}$			
Compression	0.13	0.17	0.10
G_{12} (ksi)	140	220	100
$G_{13}=G_{23}$ (ksi)	44	175	100

Table 2. Summary of strengths.

	Material		
Property	**Aμ**	**A**	**B**
$\sigma_{11} = \sigma_{22}$ (ksi)			
Tension	>50	>50	>50
Compression	4.1	8.0	5.5
σ_{33} (ksi)			
Tension	0.306	0.677	0.569
Compression	>100	>100	>100
$\sigma_{13} = \sigma_{23}$ (ksi)			
NILS(1)	0.42	2.49	0.98
OPS(2)	—	3.02	1.55

(1) Notched Interlaminar Shear (compression)
(2) Out-of-Plane Shear (V-notch beam)

The material response in all loading directions was nonlinear and listed values were determined from linear fits at small strains. Where applicable, we applied the Ramberg-Osgood relationship to model part of the nonlinear response and the corresponding fit parameters are given in this report.

The through-thickness compression and in-plane tension specimens were also subjected to cyclic loads in ranges expected in-service. Both exhibited hysteresis and strain-hardening. Furthermore, reproducible behavior was obtained only after "seasoning" the specimen by cycling several times. The through-thickness moduli were found to increase by an average of 100% after cycling to only 150 psi. These significant moduli changes could have a major effect on the acoustic transparency of the materials.

Based on both the stiffness and strength values, material A was found to be more robust than the other two materials. We also noted that the Spectra material planes appear to bond more strongly to the special material planes than to itself. This was indicated in both the notched interlaminar shear and through-thickness tension tests in which failure always occurred away from the special material layers. Consequently, the strength values measured in this study are representative of the Spectra/epoxy composite materials and it is believed that the presence of the special planes does not significantly degrade mechanical performance of any of the materials tested.

Overall, the mechanical performance of these composites is relatively poor compared with glass and carbon fiber-reinforced materials. With the exception of the in-plane tensile modulus, in-plane tensile strength, and the through-thickness compression strength, a typical pure epoxy system has higher stiffness and strength than these composites. The Spectra fabric layers compensate for these weaknesses to some degree by imparting a high degree of toughness and damage tolerance. However, the onset of damage at low stress and strain levels should be a concern for both the long-term mechanical and acoustic performance of the composites.

1. Introduction

This report summarizes the results of mechanical testing of three types of sonar window materials manufactured by two companies, referred to as A and B. Company A supplied materials with and without microspheres. The materials received were in the form of panels as described in Table 3.

Table 3. Materials list for panels received.

Panel Type	Panel ID#	Nominal Thickness (in)	Edge Dimensions (in)	Spectra Fabric Type	Micro spheres (Y/N)
A	#2	0.75	12.75x12.75	951	N
A	#3	0.75	12.75x12.50	988	Y
B	S/N 002	0.66	14.25x14.25	951	Y
B	S/N 003	0.66	12.63x12.63	951	Y

The 951 Spectra fabric is a plain weave, 0.011" thick material having 17x17 ends/in., and the 988 is a 4H satin fabric, 0.015" thick, with 32x32 ends/in. [1]. Both are woven from Spectra 1000 fiber which has presumably been plasma-treated for improved bonding to the matrix. Although little data is reported for Spectra fabric composites, a full set of in-plane properties for unidirectional Spectra 1000/epoxy was obtained from the manufacturer [2]. These properties will be useful in later comparisons to the thick sonar window materials and are summarized in Table 4.

The manufacturer's data reveals a few important points about Spectra composites. Notably, the fiber-direction moduli measured in tension and compression are significantly different. This is most likely attributable to a nonlinear behavior, especially in compression at very small strains. It has been shown that polyethylene fibers undergo compression failures at strains less than 0.1% [3] and while the fiber failure doesn't lead to complete composite failure, it does cause significant softening of the material response in compression. Also, because of this low compressive strength, which is typical for highly oriented polymeric fibers, the ultimate compression strength of the composite is similar to that of the pure epoxy matrix material. In fact, most epoxies commonly used for matrix materials exhibit higher compression strengths than the 10.5 ksi value measured for unidirectional Spectra 1000 composites.

Table 4. Properties of a unidirectional Spectra 1000/epoxy composite.

Property	Value[1]
0˚ Tensile Strength (ksi)	175
0˚ Tensile Modulus (Msi)	7.29
Longitudinal Poisson's Ratio	0.28
0˚ Tensile Strain to Failure (%)	2.63
90˚ Tensile Strength (ksi)	1.0
90˚ Tensile Modulus (Msi)	0.14
0˚ Compressive Strength (ksi)	10.5
0˚ Compressive Modulus (Msi)	2.40
90˚ Compressive Strength (ksi)	5.5
90˚ Compressive Modulus	0.37
In-plane Shear Strength (ksi)[2]	2.3
In-Plane Shear Modulus (ksi)[2]	0.12
Short Beam Shear Strength (ksi)	1.7

(1) Fiber volume fraction between 43.7 and 53.4%
(2) Iosipescu method.

The matrix-dominated strengths of the unidirectional Spectra composite are all several times smaller than typical values for carbon and glass fiber composite materials. The poorer performance of the Spectra material is most likely due to the weaker fiber/matrix bond and the presumably poor transverse properties of the Spectra fiber. Despite the tremendous tensile properties along the fiber axis, it is expected that transverse to this direction, the properties will be similar to those of unoriented polyethylene (PE). Since unoriented PE is softer than glass and carbon fiber, matrix-dominated elastic properties such as 90˚ moduli and in-plane shear modulus are also several times smaller than more traditional fiber composites.

It was expected that similar behavior would be found for the sonar window materials and that the presence of the microspheres might degrade matrix-dominated strength properties below the already low values of the fully dense material. With this in mind, test methods were developed or selected in order to avoid premature and anomalous failure modes.

After discussions with the sponsors, it was agreed that the primary goals of this effort would be:

1. Determine small-strain, elastic constants of the materials for input into acoustic and structural finite element codes. The through-thickness compression modulus and Poisson's ratios were singled out as a key properties.

2. Determine the full, nonlinear stress-strain behavior to failure. Two critical properties were defined as the in-plane compression and interlaminar shear strengths.

3. Determine the contribution of the special material planes to mechanical behavior.

4. Demonstrate, especially for the critical tests, the accuracy of the test methods using a known material.

2. Specimen Machining

Efforts were made to conserve material. With the exception of a few modifications due to minor machining and testing problems, the cutting diagram used for all three panels is shown in Figure 1.

All specimens were machined using the same techniques developed after experimentation with several types of cutting tools and processes. Specimens were fabricated by initially rough cutting the panels into strips slightly oversize in width using a waterjet machine. The waterjet was found to be the most effective way to make long cuts without delaminating the composite. The cutting parameters which yielded the best surface finish were 45 ksi water inlet pressure, 80 grit garnet, a 0.040" diameter exit orifice, and a feed rate of 5 in/min. An aluminum backing plate was used to prevent backside delamination. The waterjet cutting process did not yield square cuts due to divergence of the jet stream and a separate machining step was required to achieve final dimensions.

The strips were ground square using a surface grinder equipped with an alumina wheel and flood coolant. These strips were then cut to length using an abrasive saw and the ends were ground flat and parallel using the surface grinder. Panel B was thicker near the edges and these areas were not used to machine specimens.

All in-plane specimens were cut such that the test direction remained constant. Notches were cut using an alumina abrasive saw with a 1/16" kerf for the Notched Interlaminar Shear (NILS) specimens. The 90˚ V-notches in the bend

specimens were cut using a surface grinder on specimens held at a 45˚ orientation. The most difficult specimen to prepare and test was the In-Plane Tension (IPT) dogbone. The tapered gage section was cut on a numerically controlled (NC) mill using a left-handed fast-helix end mill. The left-handed tool was necessary to avoid the delamination which occurred with the more typical right-handed end mills.

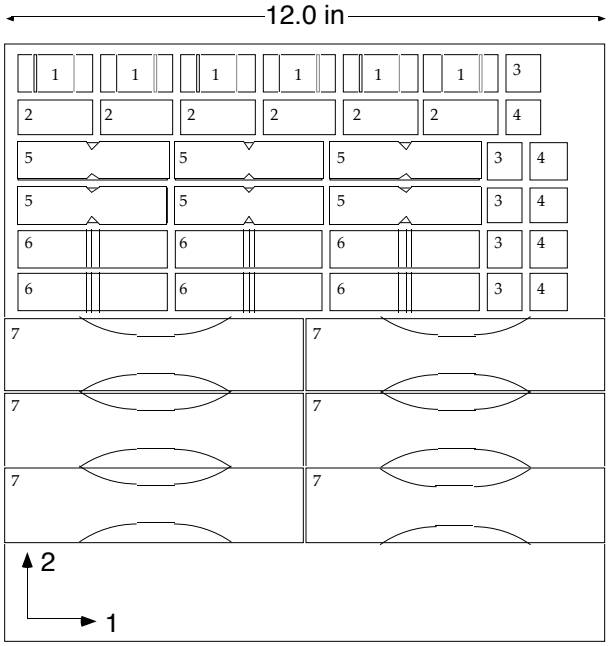

Specimens

1. Notched Interlaminar Shear (NILS)
2. 0˚ In-Plane Compression
3. Through-Thickness Compression
4. Through-Thickness Tension
5. In-Plane Shear (AFPB)(1)
6. Interlaminar Shear (AFPB)(1)
7. In-Plane Tension

(1) Asymmetric Four-Point Bend

Figure 1. Cutting diagram for all specimens tested.

3. Testing and Results

The test methods and results are reported in a manner which departs from the normal format. Rather than group all the experimental descriptions in one section and results in another, it was decided to combine the methods and results by the individual tests. Thus, the following sections are for each test type as listed in Table 5. Also given in this table are the expected properties from each test. The coordinate system used to define the various properties is shown in Figure 2.

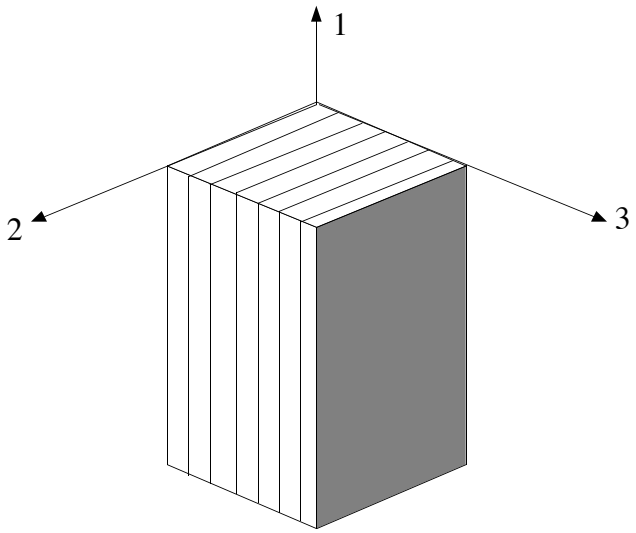

Figure 2. Coordinate definition for sonar window panels.

Table 5. Tests and corresponding properties.

Test	Elastic Constants	Strengths
Notched Interlaminar Shear (NILS)	—	$\tau_{13} = \tau_{23}$
In-Plane Compression (IPC)	$E_{11} = E_{22}$ $\nu_{12} = \nu_{21}$ $\nu_{13} = \nu_{23}$	$\sigma_{11}^{\pm} = \sigma_{22}^{\pm}$
In-Plane Tension (IPT)	$E_{11} = E_{22}$ $\nu_{12} = \nu_{21}$ $\nu_{13} = \nu_{23}$	$\sigma_{11}^{+} = \sigma_{22}^{+}$
Through-Thickness Compression (TTC)	E_{33} $\nu_{32} = \nu_{31}$	$\sigma_{33}^{\pm}$
Through-Thickness Tension (TTT)	—	σ_{33}^{+}
In-Plane Shear (IPS)	G_{12}	τ_{12}
Out-of-Plane Shear (OPS)	$G_{13} = G_{23}$	$\tau_{13} = \tau_{23}$

3.1 Notched Interlaminar Shear Strength (NILS)

Experimental (NILS)

These tests yield a value for interlaminar shear strength on a plane determined for the most part by the depth of the notches. They are essentially lap shear tests, and may be conducted in either tensile or compressive modes. We chose to run all tests in compression since it eliminates the gripping problems for thick-section composites. Specimens were notched symmetrically to generate maximum shear along the central plane. A schematic of the specimen is shown in Figure 3. The notches were held to a depth of $t/2$ +0.010/-0.000" as verified by an optical comparitor. Specimens were machined as described in Section 2. During compression, samples were supported laterally using precision V-blocks to avoid bending stresses. To minimize the friction against these supports, contact surfaces were lubricated with silicone oil. Frictional forces were measured for each test by placing the specimen slightly above the lower platen and recording the seating force. In all cases, seating forces were negligible. Stroke rate was maintained at 10^{-2} in/min for all tests. To verify the accuracy of these strength tests, 6061-T651 aluminum specimens were tested in an identical fashion.

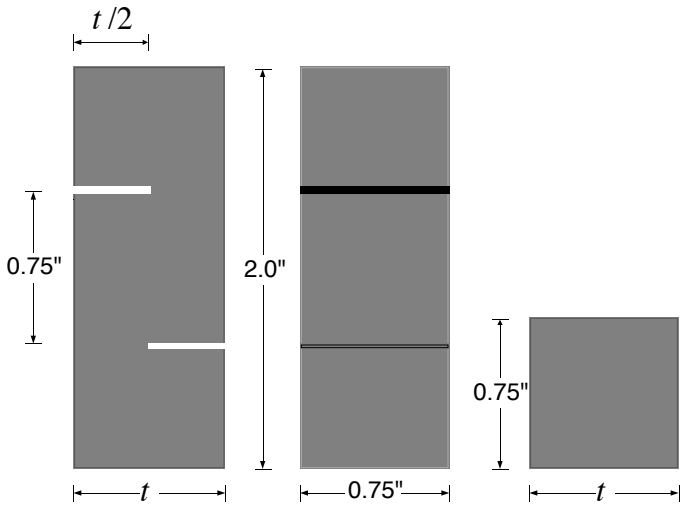

Figure 3. Notched interlaminar shear test specimen.

Results (NILS)

The results for three aluminum specimens are shown in Figure 4. The average shear strength was 31.8 ± 1.02 ksi. A published value for the shear strength of this alloy is 30 ksi [4], indicating that the test is yielding reasonable results.

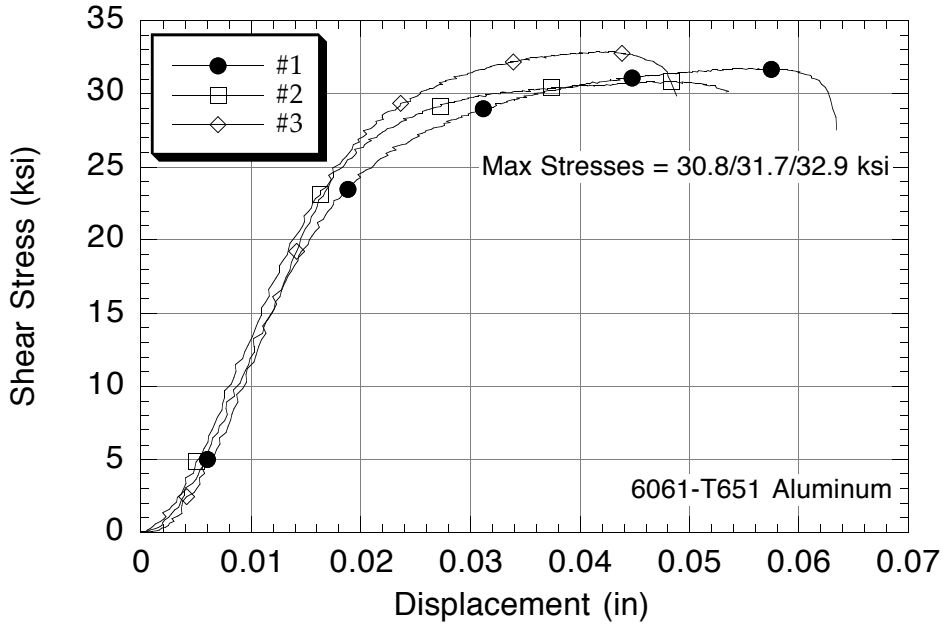

Figure 4. Notched interlaminar shear test results for 6061-T651 aluminum.

Failure of the composite specimens corresponded to a distinctive drop in shear stress to some small value, which was zero for some specimens. Some of the specimens exhibited clear cracks after the maximum stress was reached, but many appeared to undergo yielding without signs of fracture until the specimen was compressed well beyond the maximum stress level. The results for the three materials are shown in Figures 5–7 .

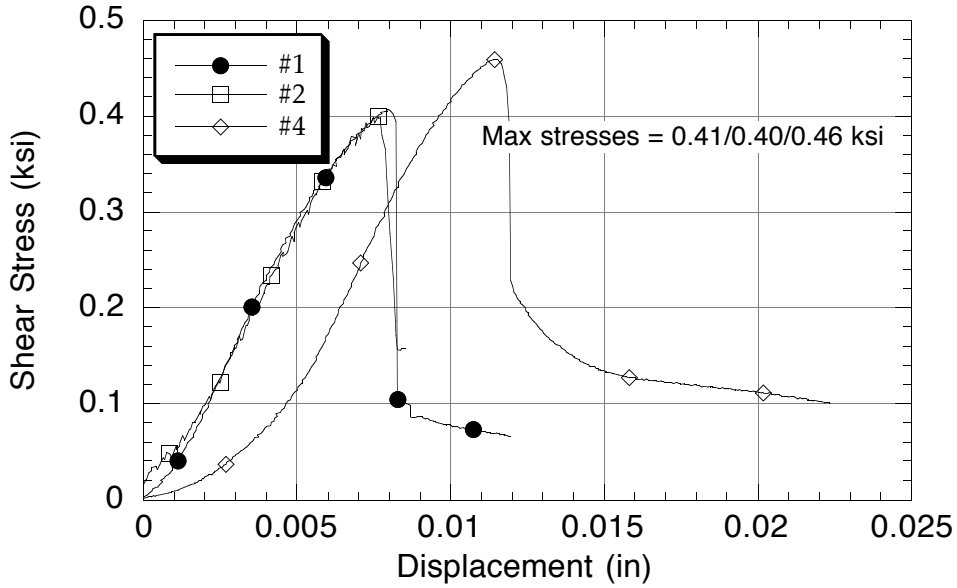

Figure 5. Notched interlaminar shear test results for Aμ.

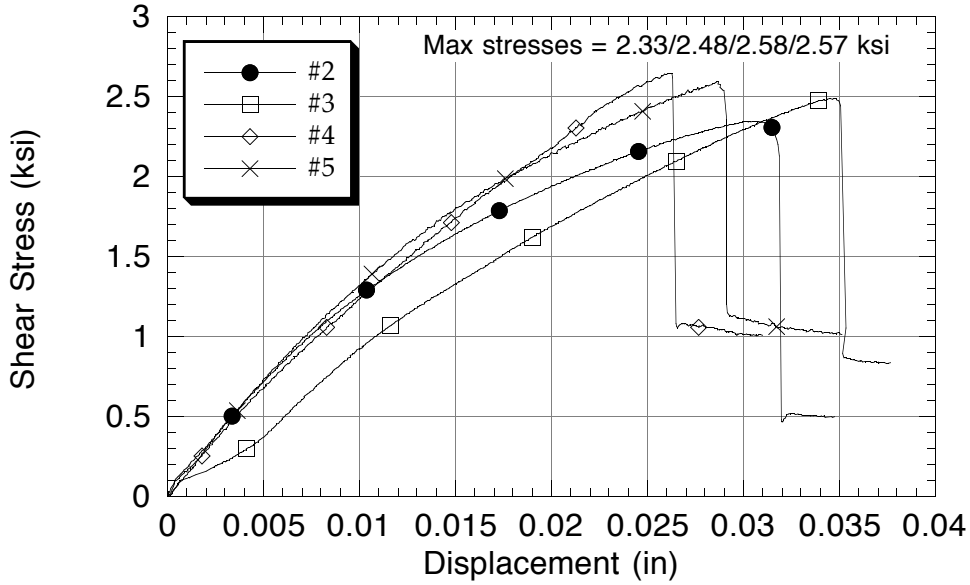

Figure 6. Notched interlaminar shear test results for A.

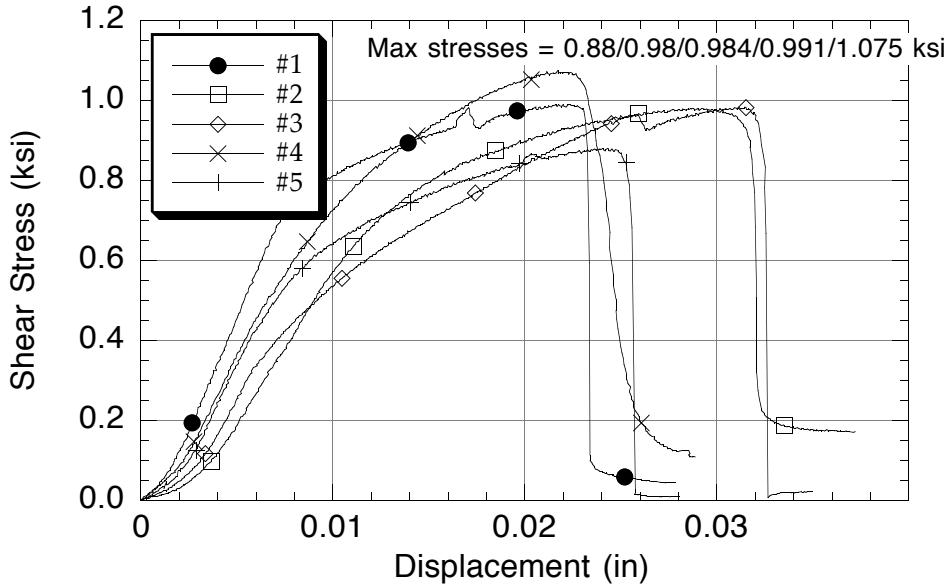

Figure 7. Notched interlaminar shear test results for B.

One sample each of materials Aμ (#3) and A (#1) were sacrificed during test set-up and check-out. A summary of the strength data from all the other tests is provided in Table 6.

Allied-Signal reports an interlaminar shear strength of 2.2 ksi for Spectra style 951 PT fabric with epoxy [1] and 1.7 ksi for unidirectional material (see Table 4), which compares favorably with the shear strength of the full-density (no microspheres) A material. The failure surface locations differed for all materials. All of the B samples failed as expected along a shear plane located in the overlap region of the notches. Breaks were relatively clean at an interface between fabric layers. Although one of the special material planes was within this region, failure always occurred away from the interface with this layer. In the A and Aμ specimens, one of the special material planes is located within the notch overlap region, yet failure never occurred along an interface with these planes. Instead, these materials always failed just outside the overlap region and in multiple planes, indicating the Spectra fabric layers are more strongly bonded to the special material layers than to themselves.

Table 6. Interlaminar shear strength data.

Material	Specimen	Interlaminar Shear Strength (ksi)
Aμ	1	0.41
Aμ	2	0.40
Aμ	4	0.46
Aμ	Average (SD)	**0.42** (0.032)
A	2	2.33
A	3	2.48
A	4	2.58
A	5	2.57
A	Average (SD)	**2.49** (0.12)
B	1	0.88
B	2	0.98
B	3	0.98
B	4	0.99
B	5	1.08
B	Average (SD)	**0.98** (0.069)

3.2 In-Plane Compression (IPC)

Experimental (IPC)

For in-plane compression tests, rectangular specimens approximately 1.5"x3/4"x *t* were fabricated. Normally direct compression of rectangular prism fiber composite specimens results in end failures such as brooming and a preliminary test of a sonar window composite confirmed that this material behaved similarly. To generate a gage failure, all specimen ends were potted with epoxy in aluminum end caps as shown in Figure 8. After curing the epoxy, the specimens were held by the gage section while the aluminum ends were ground flat and parallel to the specimen axes.

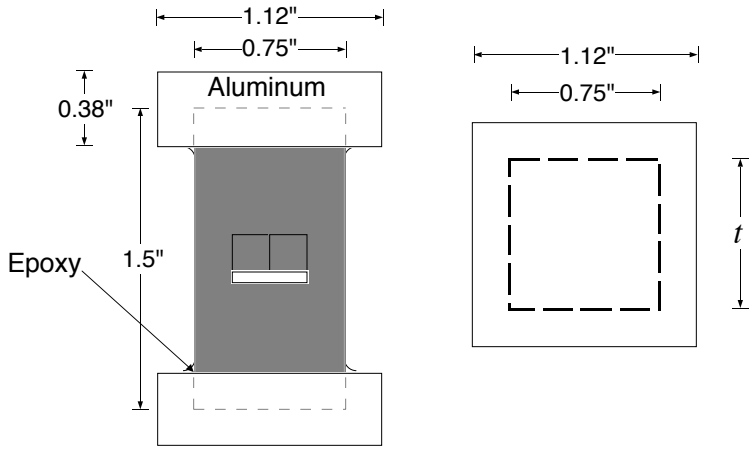

Figure 8. In-plane compression test specimen.

Each specimen was fitted with four biaxial strain gages (Measurements Group CEA-09-1250T-350) on the four lateral surfaces. These were used to determine compression stress-strain behavior as well as the Poisson's ratios. The gages were consistently labelled as shown in Figure 9.

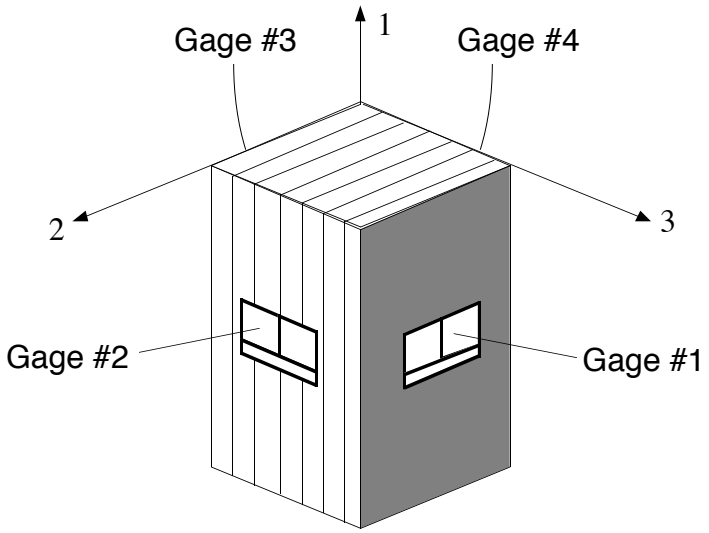

Figure 9. Material planes and gage placement.

Compression tests were conducted using an MTS servohydraulic test machine equipped with a precision subpress having platens ground parallel to within 50 μinches. Load was measured using a 55 kip load cell calibrated to NIST standards. To guarantee parallelism of the specimen ends, each was lapped in the subpress using 240 grit abrasive paper, thus yielding end surfaces which parallel to within 0.0003". Load, stroke, and strain gage data were acquired using a National Instruments LabView data acquisition system with 12-bit accuracy. For all tests, the stroke rate was 10^{-2} in/min., yielding a strain rate of ca. 10^{-4} s^{-1}. All tests were run at least until a maximum load was reached and the specimen showed visible signs of failure.

Results (IPC)

Aluminum Calibration Specimen: In order to test the ability of the compression test set-up to accurately determine material properties, a compression test of a 6061-T651 aluminum sample was run in exactly the same manner used for all the sonar window materials tests. This sample was thus potted into aluminum endcaps with epoxy and ground in the surface grinder and lapped just prior to testing using abrasive paper in the subpress. For these tests, the primary concern was simply the uniformity of loading. Consequently, only axial gages (rather than the biaxial gages used for the sonar window materials, where Poisson data was also desired) were mounted on the four lateral surfaces. Repeated loading to stress levels of about 25 ksi demonstrated that agreement between the four gages was excellent. An example of the stress versus the four axial gage outputs is shown in Figure 10. The average modulus of these data was determined from a linear least squares fit to be 10.1 Msi, which corresponds to published values for

this alloy [4]. A more concrete demonstration of the uniformity of the applied load is the plot of percentage variation of strain (with respect to the average value) versus stress as shown in Figure 11. The difference between gages is a fixed amount for the entire loading and this yields a decreasing percentage variation with strain. At the higher strain levels the gages agree within 5%.

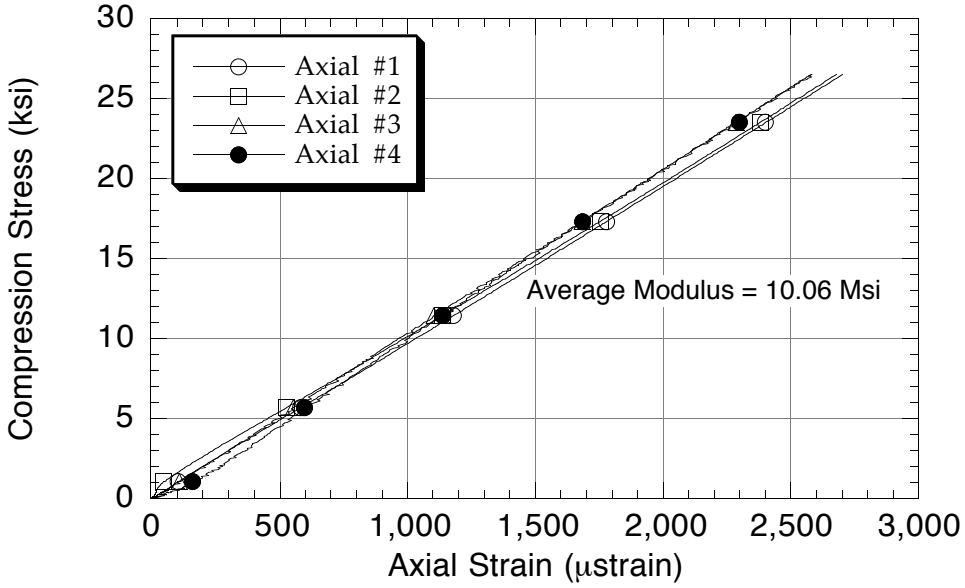

Figure 10. Stress versus strain output of all four gages for 6061-T651 aluminum in compression.

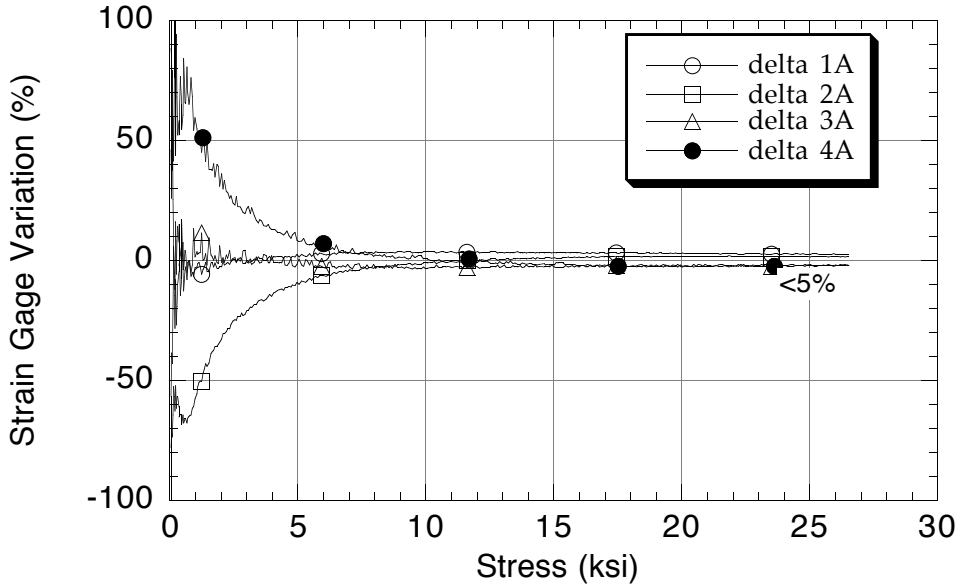

Figure 11. Axial strain gage variability in compression test of 6061-T651 aluminum.

Constitutive Behavior: Plots of stress versus the average axial strain for the three materials are shown in Figures 12–14. Linear elastic behavior was only observed for strains below ca. 0.01%. Linear fits to this region of strain yielded the initial moduli values listed in Table 7.

Table 7. Initial in-plane compression moduli.

Material	Specimen	$E_{11} = E_{22}$ (Msi)
Aμ	1	2.58
Aμ	2	2.44
Aμ	3	2.70
Aμ	Average (SD)	**2.60** (0.13)
A	1	4.17
A	2	3.93
A	3	4.02
A	Average (SD)	**4.00** (0.12)
B	1	3.39
B	2	3.26
B	3	3.22
B	Average (SD)	**3.30** (0.09)

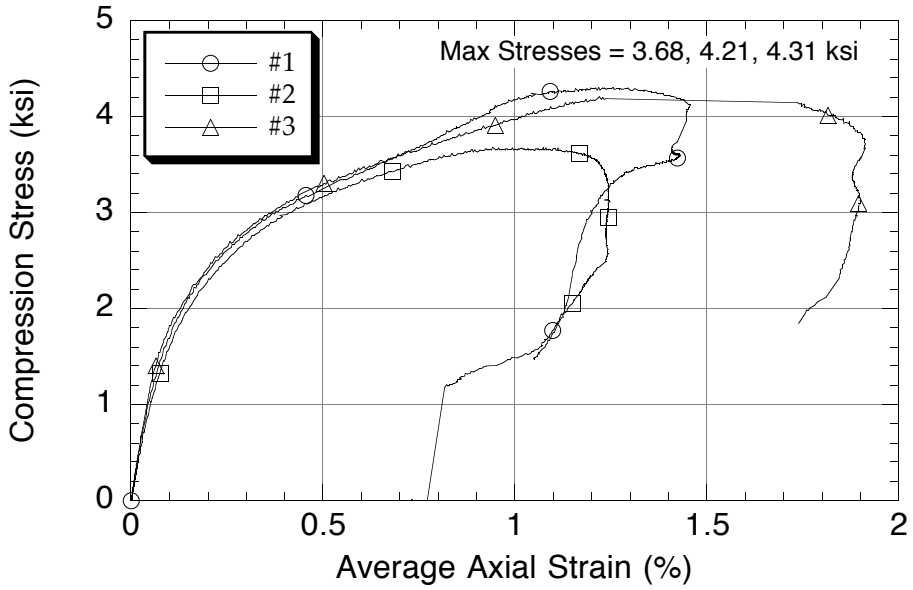

Figure 12. In-plane compression response of Aμ.

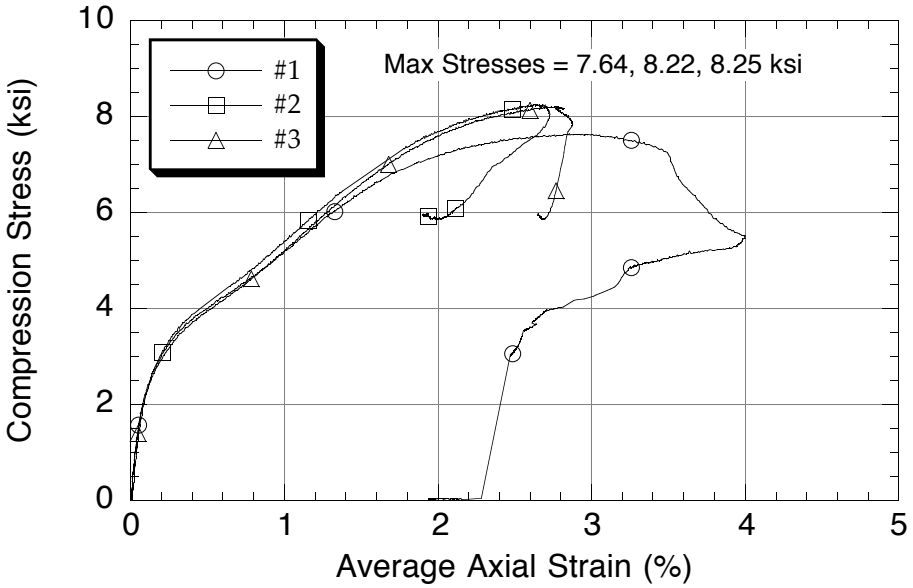

Figure 13. In-plane compression response of A.

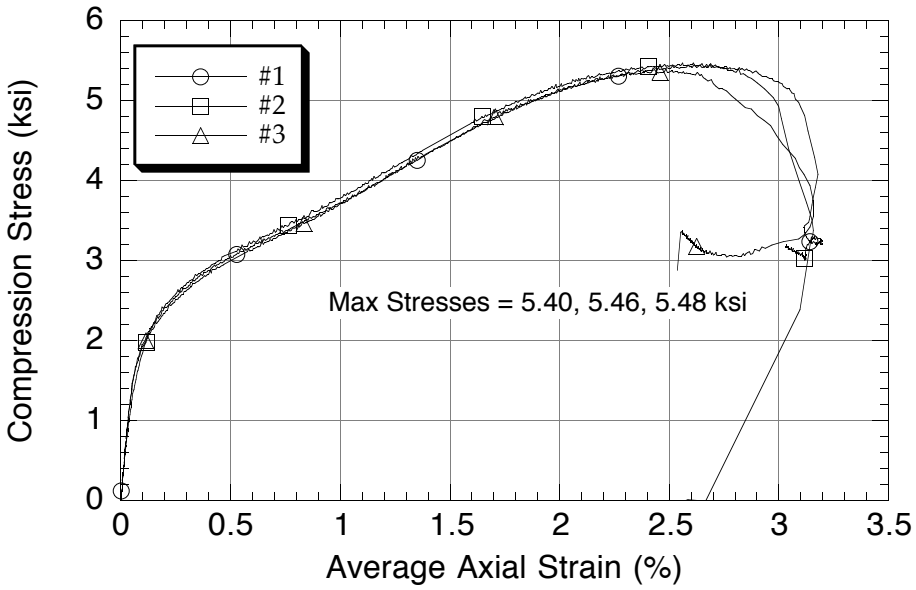

Figure 14. In-plane compression response of B.

As stated earlier, it is known that the Spectra polyethylene fiber fails in compression at relatively low strain levels [3]. Presumably, the nonlinear compression behavior is due in part to the accumulation of this fiber damage with strain. Because of the nonlinear nature of most of the stress-strain response, we applied a Ramberg-Osgood 3-parameter fit, which is defined by

$$\varepsilon = \frac{\sigma}{E}\left[1+\left(\frac{\sigma}{\sigma_o}\right)^{\beta \pm 1}\right]$$

where ε is strain, σ is stress, E is the initial Young's modulus, and σ_o and β are constants. Data was fit only up to 0.4% strain. The fit could be applied to past this level for some samples, but for others there was an inflection in the curve which occurs just beyond this strain level. The fit parameters are summarized in Table 8. Specimen #2 (A) was tested first and was used to check the test set-up by cycling two times to low stress levels before taking it to failure.

Table 8. Ramberg-Osgood fit parameters for in-plane compression.

Material	E_{11}=E_{22} (Msi)	σ_o (ksi)	β
Aμ	**2.5** (0.23)	2.3 (0.07)	3.9 (0.11)
A	**3.7** (0.27)	2.7 (0.21)	4.1 (0.20)
B	**3.4** (0.57)	2.1 (0.21)	5.0 (0.35)

The quality of these fits is demonstrated by comparing the Ramberg-Osgood curves generated from the average values in Table 8 against the data from all three specimens of each material. These are shown in Figures 15–17 for the three materials.

Comparison of the initial Young's moduli obtained from the linear fit below 0.01% strain and the Ramberg-Osgood fit up to 0.4% strain shows that there is reasonable agreement between the two methods. Therefore, the nonlinear fit does a sufficient job of capturing the small strain behavior.

For comparison, Allied-Signal reports a flexural modulus value of 2.0 Msi for Style 951 PT plain weave fabric at 65% fiber volume in an epoxy matrix [1]. While this is slightly lower than values measured here, it should be noted that some discrepancies are likely due to the differences in defining initial moduli values for a material which exhibits a highly nonlinear response.

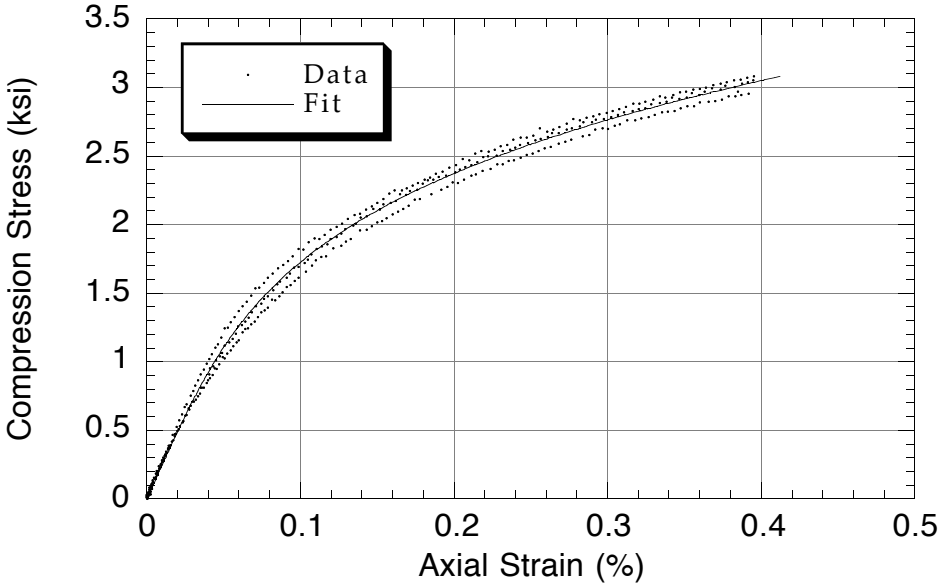

Figure 15. Ramberg-Osgood Fit to all Aμ in-plane compression specimens.

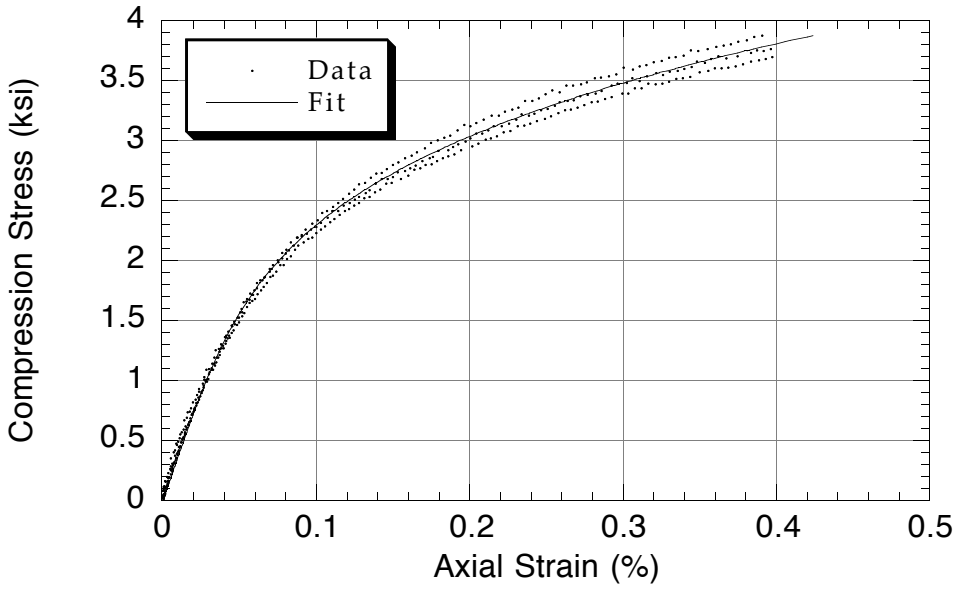

Figure 16. Ramberg-Osgood Fit to all A in-plane compression specimens.

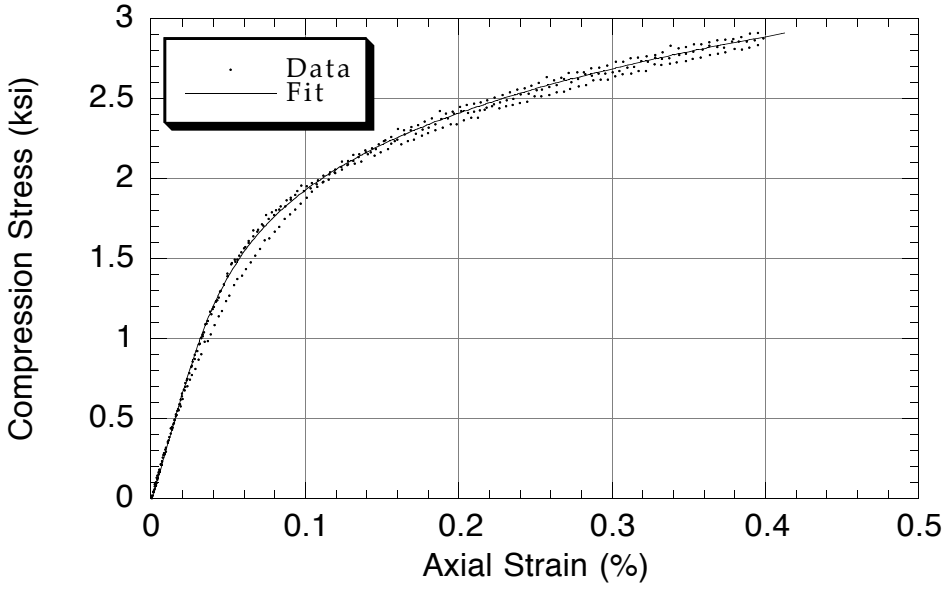

Figure 17. Ramberg-Osgood Fit to all B in-plane compression specimens.

In order to compare properties of the three types of materials, the average Ramberg-Osgood fits are plotted together in Figure 18.

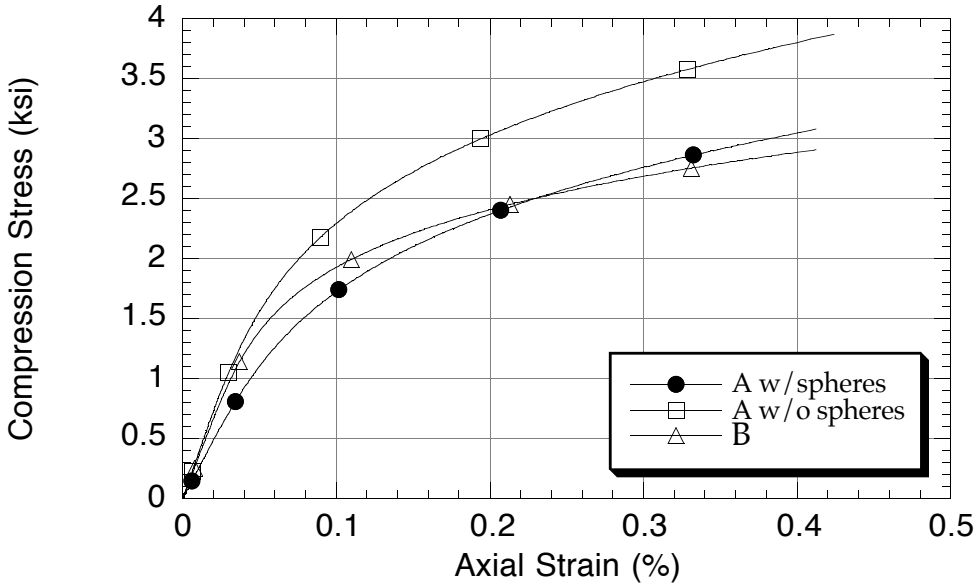

Figure 18. Ramberg-Osgood Fits to the three materials under in-plane compression.

The four lateral surfaces of a specimen yield two measurements each of the two different Poisson's ratios determined from edge (1-3) and face (1-2) planes. All tests showed that the relationship between transverse and longitudinal strains was nonlinear. Corrections made for the transverse strain sensitivity of the gages were most significant for the transverse gages on the 1-2 planes. Examples of the Poisson's response are shown in Figures 19 and 20 for the 1-2 and 1-3 planes, respectively of panel B. In order to capture the small-strain behavior, two different "Poisson's ratios" were determined for each pair of gages. These ratios were taken from least squares linear curve fits from the 0–0.05% and 0.05–0.5% compression strain ranges. Results are summarized below in Tables 9 and 10. Poisson's ratios for both materials A and B varied by 10–15%, while the values for material Aμwere much more inconsistent and varied by 20–50%. This is most likely due to local material variability and the initiation of damage at small strains in this weak material.

Table 9. Poisson's ratios measured in the 0–0.05% strain range.

Material	Specimen	ν_{12} (Gage #1)	ν_{12} (Gage #3)	ν_{13} (Gage #2)	ν_{13} (Gage #4)
Aμ	1	0.184	0.267	0.251	0.352
Aμ	2	0.176	0.167	0.382	0.302
Aμ	3	0.183	0.243	0.492	0.484
Aμ	Average (SD)	**0.20** (0.041)		**0.38** (0.097)	
A	1	0.105	0.095	0.601	0.510
A	2(1)	0.121	0.104	0.625	0.460
A	3	0.102	0.101	0.609	0.476
A	Average (SD)	**0.10** (0.009)		**0.55** (0.073)	
B	1	0.105	0.137	0.693	0.602
B	2	0.097	0.081	0.724	0.549
B	3	0.083	0.098	0.626	0.611
B	Average (SD)	**0.10** (0.020)		**0.63** (0.064)	

(1) Taken from the third loading of the specimen.

Table 10. Poisson's ratios measured in the 0.05% – 0.5% strain range.

Material	Specimen	ν_{12} (Gage #1)	ν_{12} (Gage #3)	ν_{13} (Gage #2)	ν_{13} (Gage #4)
Aμ	1	0.109	0.196	0.180	0.288
Aμ	2	0.083	0.059	0.328	0.440
Aμ	3	0.051	0.126	0.358	0.385
Aμ	Average (SD)	**0.10** (0.053)		**0.33** (0.090)	
A	1	0.067	0.065	0.502	0.421
A	2[(1)]	0.070	0.060	0.445	0.355
A	3	0.061	0.058	0.414	0.377
A	Average (SD)	**0.06** (0.005)		**0.42** (0.052)	
B	1	0.048	0.055	0.538	0.517
B	2	0.038	0.042	0.605	0.508
B	3	0.042	0.049	0.577	0.620
B	Average (SD)	**0.05** (0.006)		**0.56** (0.047)	

(1) Taken from the third loading of the specimen.

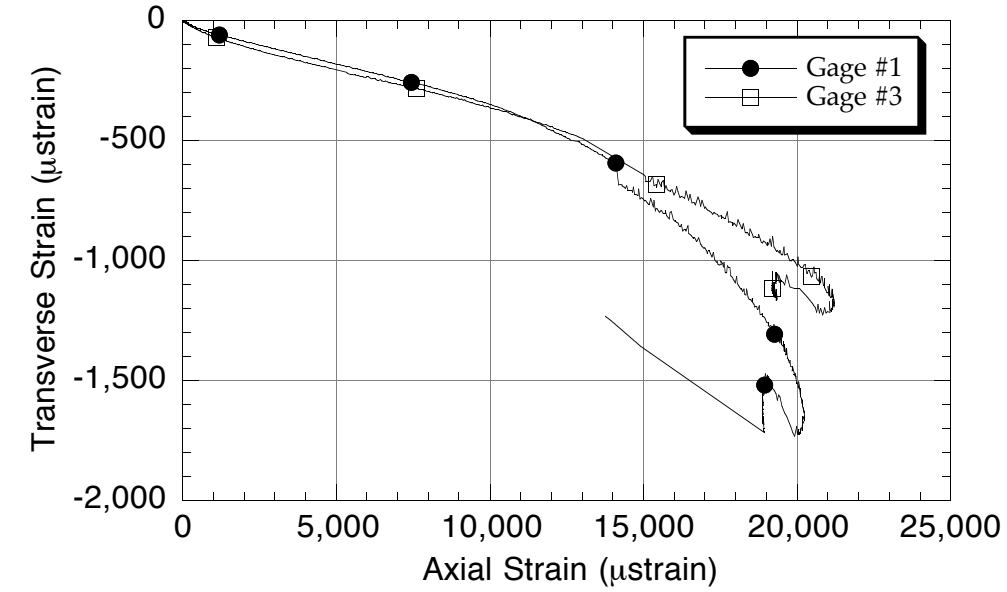

Figure 19. 1-2 plane Poisson's effect for B under in-plane compression.

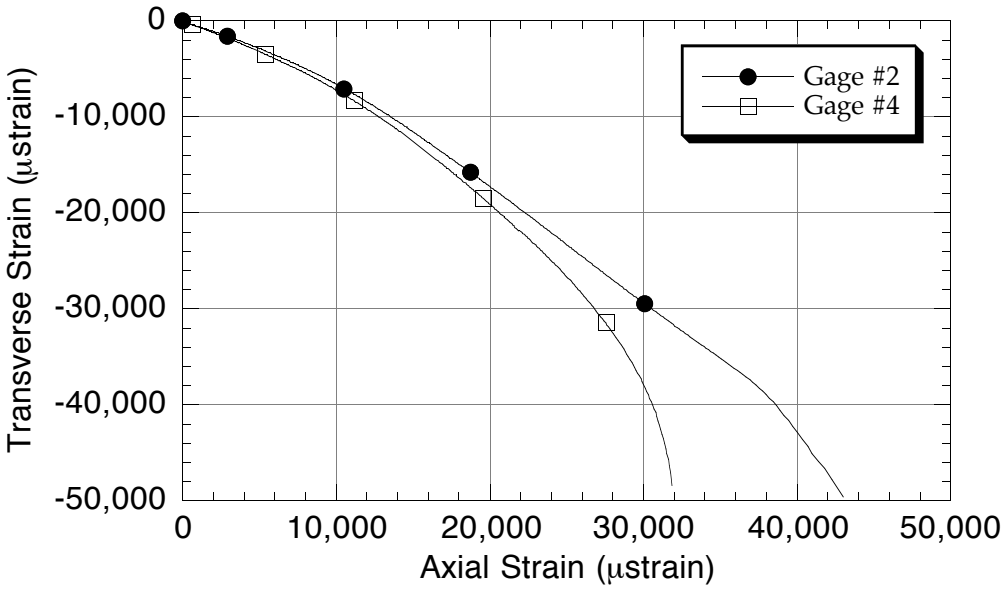

Figure 20. 1-3 plane Poisson's effect for B under in-plane compression.

Failure: Failure of all specimens was a gradual process of compression kink band formation which became noticeable after the stress had reached a peak value. At high compressive strains and after the kink bands had formed, layers began to delaminate. All the kink bands were formed via shearing in the interlaminar mode, thus the obliquely oriented band is on the fabric layer edge surface (the 1-3 plane). For materials Aμ and B, the band formed away from the bonded ends of the specimen. Failure of all the higher strength A specimens appeared to have initiated at one potted end. Kink bands were relatively well-defined for the A and B specimens, but much less so for the Aμ samples. The latter also showed more delaminations than the other two materials and in two of the three tests a delamination occurred at the darkest special material layer.

A summary of the maximum stresses and kink band angles is given in Table 11. The angle is measured with respect to the loading direction. The 8 ksi strength measured for the A panel is close to the 10.5 ksi value measured for unidirectional material (Table 2). Although the sonar material is basically a 0/90 lay-up which has only half the fiber in the load direction, it has similar compression strength to a unidirectional lay-up.

Table 11. In-plane compression strength data.

Material	Specimen	Strength (ksi)	Kink Angle (°)
Aμ	1	3.68	45
Aμ	2	4.21	*(ill-defined)*
Aμ	3	4.31	50
Aμ	Average SD	**4.1** (0.34)	
A	1	7.64	45
A	2(1)	8.22	42
A	3	8.25	42
A	Average SD	**8.0** (0.34)	
B	1	5.40	36
B	2	5.46	37
B	3	5.48	37
B	Average SD	**5.5** (0.04)	

(1) Taken from the third loading of the specimen.

3.3 In-Plane Tension (IPT)

Experimental (IPT)

The one case where the properties of the Spectra fiber are of high performance caliber is tension in the fiber direction. As shown in Table 4, the unidirectional material has a strength of 175 ksi and the sonar fabric composites are expected to have about half of this tensile strength. Considering the thickness of the sonar panels, this is by far the most difficult test for obtaining strength data. Standard composite tensile specimens are loaded by shear through end-bonded tabs. These specimens are typically long (ca. 9") to allow sufficient shear-lag build-up of stress from the gripped ends to the gage section. Specimens are also typically thin (0.05-0.1"), which helps the transfer of shear to pure tensile loads.

The sonar panels are particularly challenging for several reasons. They are much thicker than the standard specimens; since the goal of this project is to determine the properties of the entire panel, including the special material planes, the whole thickness is required in the specimen. As the data in Table 4 show, the shear moduli and shear strengths of the Spectra composites are relatively low, requiring even larger length specimens to achieve complete transfer of grip stresses into a homogeneous tensile stress in the gage section. The problem is further compounded by the poor stiffness and strength properties in every direction other than fiber tension.

We decided that given the constraints of the specimen size (full panel thickness and maximum length 12") that little stress could be transferred by simply gripping the faces of the material. This would simply result in a very nonhomogeneous stress and strain distribution where the outer layers of the panel would be the most highly tensioned and the inner layers would be hardly deformed. It was instead decided to design a specimen which would at least yield valid stress-strain data up to stress values corresponding to the magnitude of the in-plane compressive strengths. Considering that the compressive side of the strongest panel fails at 8 ksi, we targeted at least double this or 20 ksi as the goal for obtaining stress-strain tensile data.

The specimen design is basically a 6" long dogbone shape as shown in Figure 21. The radius of the transition region is 3.708" and the gage length is 0.75". The gage length could have been increased by as much as 6", but it was felt that material should be conserved and, for the purposes of collecting data up to 20 ksi tension stress, that the overall 6" long specimen would suffice.

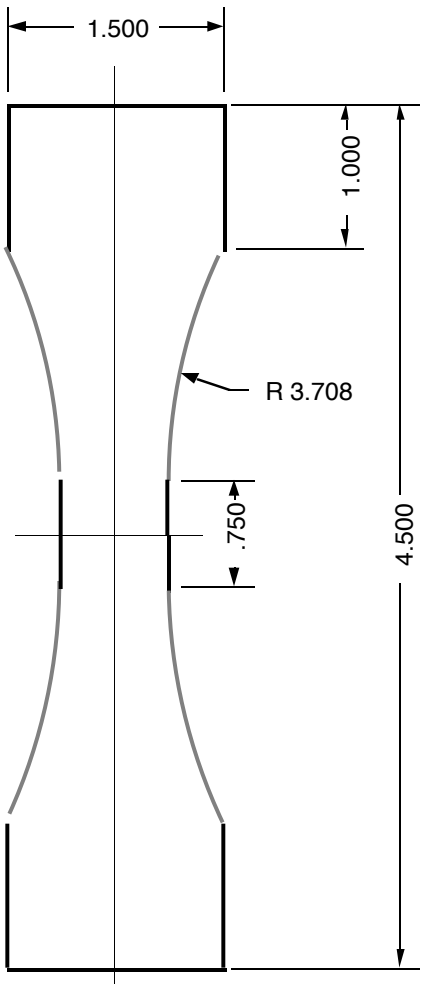

Figure 21. In-plane tension test specimen. All dimensions in inches.

Special grips were designed to use as much of the specimens ends to transfer load into the gage section as shown in Figure 22. All four surfaces are gripped, but most of the load is transferred along the shoulders of the dogbone. The lateral faces of the sample are clamped with a retainer plate. In addition to transferring load, the grip was designed to prevent any motion of the specimen end by containing it volumetrically. Given the generally poor properties of the Spectra composite, it was felt that the significant loads required to generate tensile failure could only be sustained if the ends of the sample were subjected to triaxial compression by rigid confinement. The matching retainers and retaining plates were machined from aluminum and, to prevent lateral motion of the grips due to high stresses on the shoulder support, the entire clamped end was gripped in 500 kip wedge fixtures as shown in Figure 22.

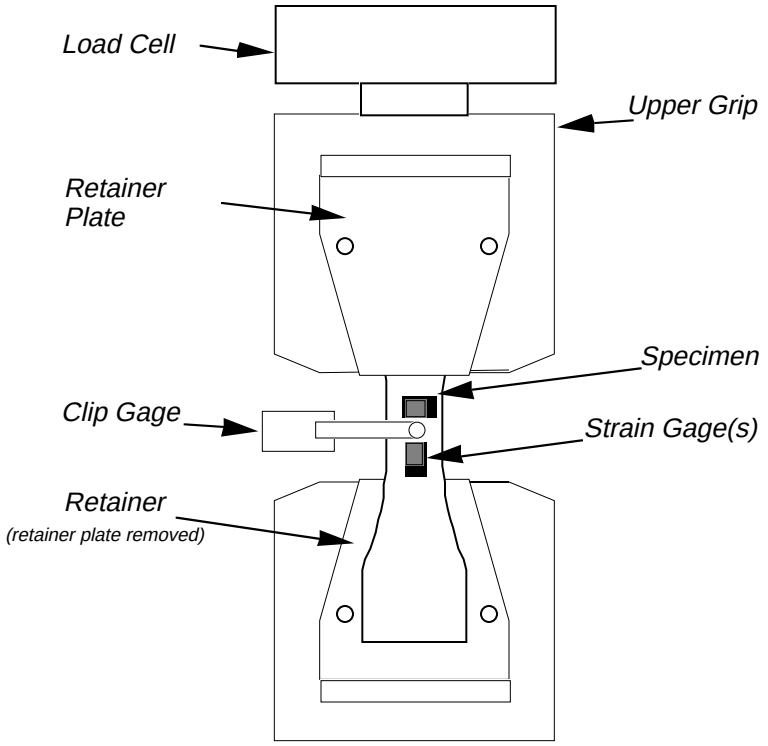

Figure 22. In-plane tension test set-up.

Strains on the two different faces of the gage length were measured using foil strain gages (either two Measurements Group EA-06-090EG-350 gages or a stacked CEA-13-125WT-350) and an extensometer (clip gage). For some reason, possibly the rougher surface finish left by the end mill, we were unable to bond strain gages to the face formed by the edges of the panel (the 1-3 plane). The lateral displacement in this plane was therefore measured via a clip gage as shown in Figure 22. Transverse and longitudinal strains were measured on the two opposing 1-2 planes using strain gages. The gages were calibrated against a shunt resistor in the bridge. The clip gage was calibrated using a digital micrometer.

Initial attempts to generate successful tensile failures exposed problems with containing the ends of the dogbone specimen. Our initial lateral containment scheme, consisting of through bolts connecting the aluminum alloy retainer plates proved inadequate. Sufficient force was generated during the test to strip the threads on the back retainer plate (even after installation of a Helicoil insert), thus compromising containment. Test specimens were observed to "extrude" through a gap which developed between the retainer/retainer plate. Attempts to bolster lateral containment through addition of external clamping force proved marginally effective. It was decided at this point that the limited potential value of tensile ultimate failure data did not justify the additional cost to manufacture

more robust fixturing. The remaining three samples, one of each panel, would be tested for initial stress-strain behavior as described below. Given the time and resources, it is believed that a tensile failure could be obtained using steel retainer plates.

Tensile tests on the remaining specimens were conducted on a 500 kip MTS servohydraulic test machine equipped with an electronically calibrated 50 kip load cell. All specimens were subjected to three tests in load control, consisting of two cycles from 0 to 5,000 lb at 1,000 lb/min and a final cycle of 0 to 10,000 lb at 2,000 lb/min. For the typical dimensions of the specimens, these tests corresponded to cycling up to 10 and 20 ksi, respectively.

Results

Constitutive Behavior: An example plot of cyclic stress versus the average axial strain for the Aμspecimen is shown in Figure 23. The response changed with each cycle as the material underwent strain-hardening and this is representative of the behavior observed for all three composites. The settling of the sample into the fixturing disturbed the beginning of the stress-strain curve, especially on the first cycle. Modulus values and the two Poisson's ratios were measured using linear fits on the initial part of the third cycle response curves and are summarized in Table 12. This data is considered less reliable than the corresponding in-plane compression values because a substantial load was required to seat the specimen in the grips and achieve uniform loading in the gage section. As a result, much of the data at low stress levels (<2 ksi) is masked by grip effects. In general, the behavior was relatively linear after the cycling, although there was some strain-softening at the higher stress levels. After the three cycles, all three specimens were pulled to "failure," which in all cases corresponded to problems with gripping. In this way, it was established that the lower bound on the tensile strength of these materials is 50 ksi.

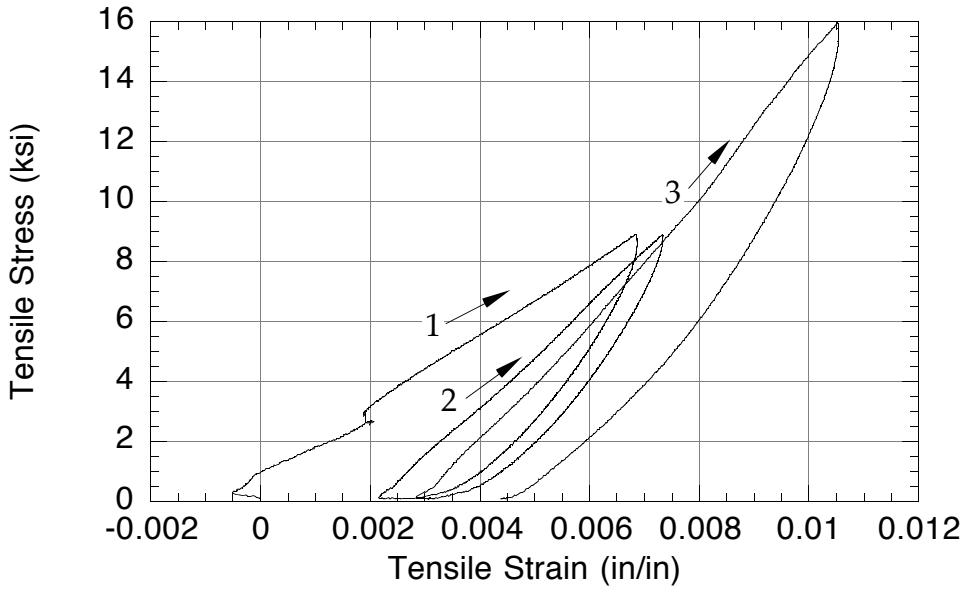

Figure 23. In-plane cyclic tension of Aμ.

Table 12. Initial moduli and Poisson's ratios from in-plane tension tests.

Material	$E_{11} = E_{22}$ **(Msi)**	ν_{12}	$\nu_{13} = \nu_{23}$
Aμ	2.0	0.15	0.54
A	2.9	0.06	0.35
B	1.9	0.06	0.65

3.4 Through-Thickness Compression (TTC)

Experimental (TTC)

For through-thickness compression tests, rectangular specimens were ground square and parallel to dimensions 0.5" x 0.5" x *t*, the panel thickness. A minimum of material was ground from the thickness direction to make the end faces parallel. Initial tests with these samples were run to determine failure loads and in all cases the capacity of the test machine was exceeded before failure. Based on the maximum loads achieved, it was established that the through-thickness compression strength of all three materials is greater than 100 ksi. All further efforts were devoted to measuring the stress-strain response at practical stress levels.

Initial attempts to measure strains with biaxial gages mounted on all four sides of a larger specimen with dimensions 0.75" x 0.75" x *t* were unsuccessful. Strains from the four axial gages were wildly different and in some cases of opposite sign. Gages also debonded or gave erroneous readings after relatively small strains. Previous work in our lab has shown that gages bonded to the edges of laminates suffer from premature failure and for the Spectra composites it appears to be a more severe problem. To circumvent this problem, it was decided that average axial and transverse strains would be measured using clip gages. One gage was mounted to two opposing sides of the specimen to measure lateral displacements. Another gage was mounted to the loading platens to measure longitudinal displacement. Both gages were calibrated against a digital micrometer.

The tests were conducted using a small precision subpress in Model 1125 Instron test machine. Because material response in the small stress and strain regime is important for acoustic properties, most of the loading was kept below 400 psi. The weight of the piston loading the specimen was just under 1 lb, corresponding to an initial preload of approximately 4 psi in each test. All tests were conducted at a stroke rate of 0.001 in/min. Each specimen was cycled between 0 and 160 psi several times and 0 and 400 psi one time. A schematic of the set-up is shown in Figure 24.

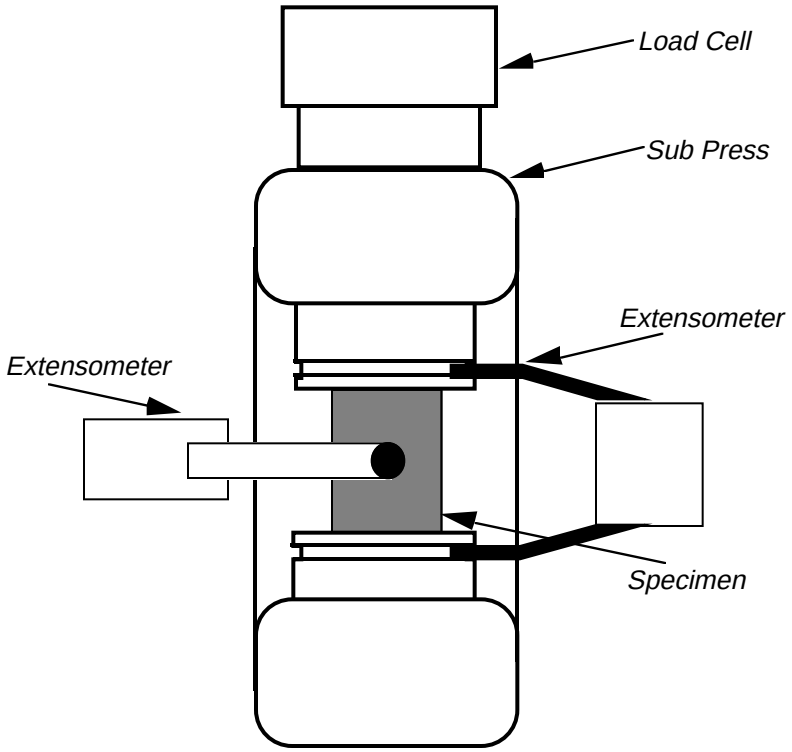

Figure 24. Test set-up for through-thickness compression.

Results (TTC)

Constitutive Behavior: The most significant result of the through-thickness compression behavior is the large change in the material response with cycling at relatively low stress levels. Examples for the three different materials are shown in Figures 25–27. The initial loading is much different than subsequent cycles with the materials appearing much softer in the first cycle. Behavior seems to become repeatable after the first cycle and although there is hysteresis, the samples always returned to the original length. Even after cycling, the stress-strain curve shows some strain hardening. However, there is a distinct slope change when the stress reaches the maximum of the previous cycle. Reproducible behavior below a fixed stress level can be achieved after "seasoning" or cycling the materials to this level. The relative change in through-thickness modulus between the first and subsequent cycles was greatest for materials A and B. Although the percentage increase varied widely, changes on the order of 100–200% were measured for these materials. The Aμ materials showed modulus increases of about 50% after the initial loading to 160 ksi.

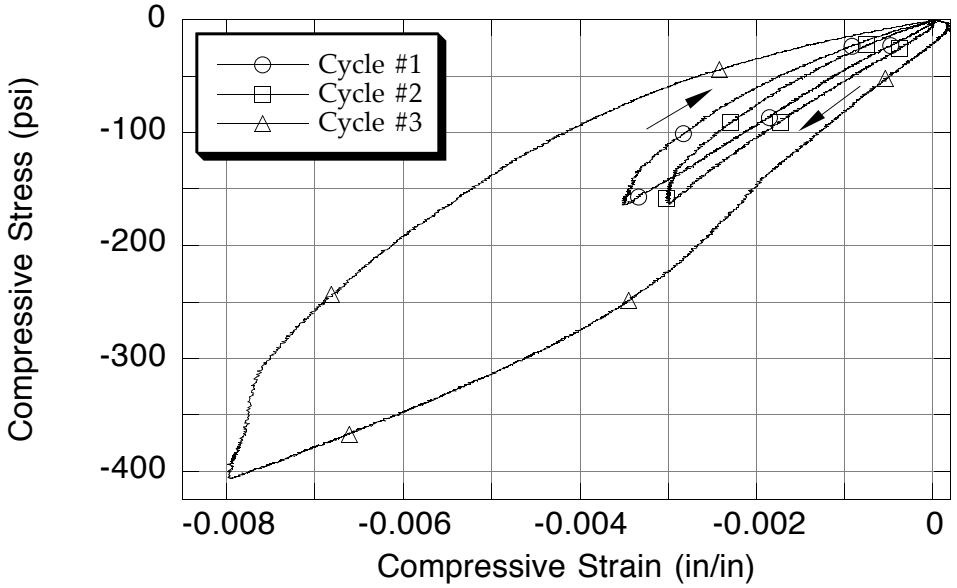

Figure 25. Through-thickness cyclic compression of an Aμ specimen.

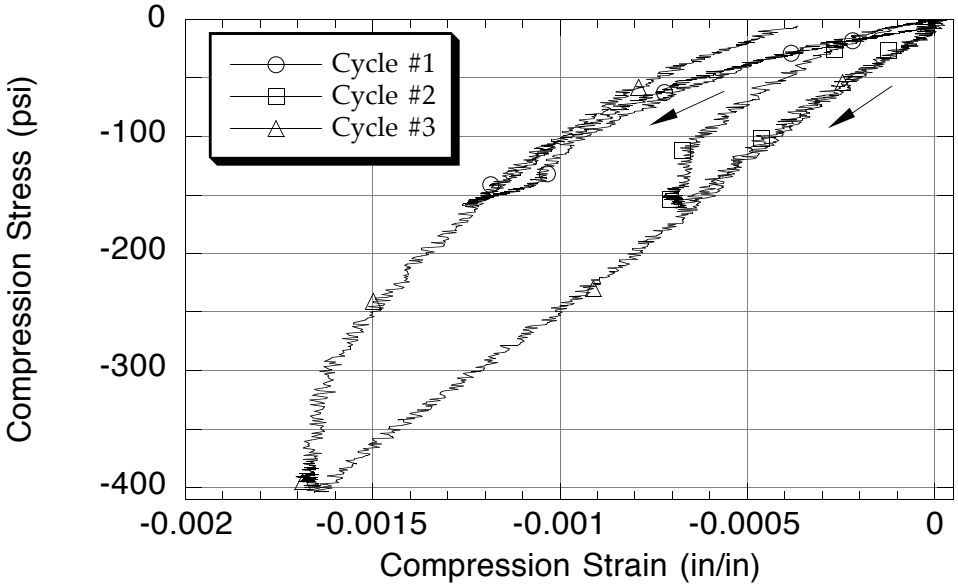

Figure 26. Through-thickness cyclic compression of an A specimen.

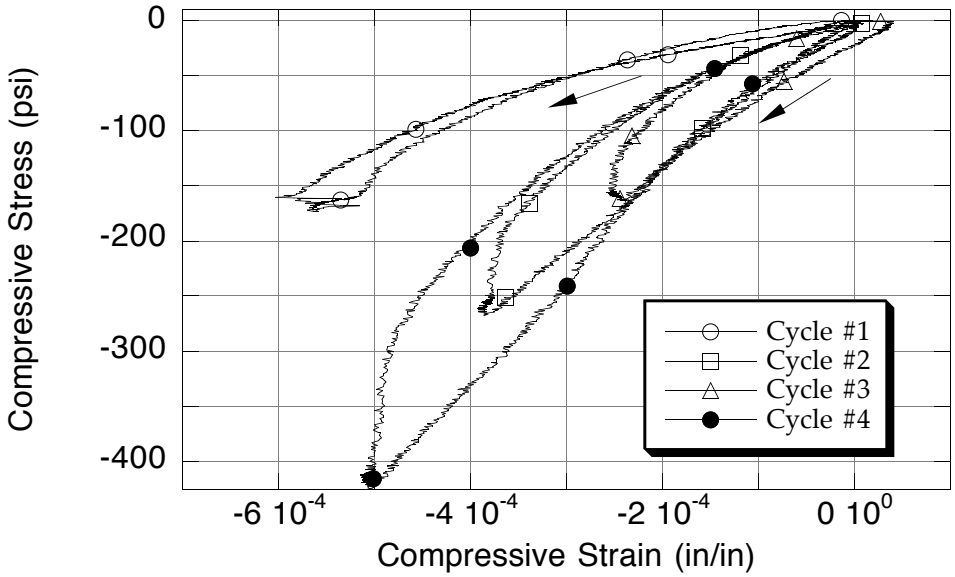

Figure 27. Through-thickness cyclic compression of a B specimen.

To check for differences between the 1- and 2-directions, the clip gage measuring lateral deformation was placed in both directions after the sample was initially cycled. No significant difference in the Poisson's behavior was noted, indicating that the two in-plane directions are equivalent as assumed. The elastic constants measured after each specimen was cycled at least three times to 160 ksi compression stress are summarized in Table 13. The Poisson's ratios are relatively small as expected for compression transverse to the fiber directions. The elastic modulus of the B material was found to be several times greater than both the A materials.

Table 13. Elastic constants for through-thickness compression tests measured after cycling three times to 160 psi.

Material	Specimen	E_{33} (ksi)	$\nu_{31} = \nu_{32}$
Aμ	4	142	0.15
Aμ	5	62	0.10
Aμ	Average (SD)	**100** (57)	**0.13** (0.035)
A	3	165	0.19
A	4	220	0.15
A	Average (SD)	**190** (39)	**0.17** (0.028)
B	4	553	0.12
B	5	788	0.11
B	6	633	0.08
B	Average (SD)	**660** (119)	**0.10** (0.021)

3.5 Through-Thickness Tension (TTT)

Experimental (TTT)

These tests were conducted to determine the transverse tensile strength only. There was interest in seeing if the special material planes would be more poorly bonded than the rest of the laminate. For the B panel, the special planes are distributed throughout the thickness and some are located very close to the surface. Therefore, the test specimen had to be designed so that it would put the entire panel thickness under a uniform tensile stress. This constraint naturally ruled out the first choice for these specimens, which is a dogbone shape with a reduced gage section.

The only option available was to bond the ends of samples directly to metal endpieces and hope that the butt tensile strength of this adhesive joint was greater than the through-thickness strength of the laminates. Preliminary tests confirmed that failure in the composite could be achieved. The sample was machined and ground to a cube 0.75" x 0.75" by *t*, the thickness of the panels. These were bonded to cylindrical endplugs slightly greater than 1" in diameter. This diameter was matched to the diagonal of the composite specimen so that it could be easily centered during bonding. The endplugs had threaded holes on the opposite ends for attachment to test machine fixturing. To minimize bending stresses, universal joints were used at both ends of the specimen. All tests were conducted at a nominal stroke rate of 0.05 in/min using a model 1125 Instron test machine equipped with a 2 kip load cell, which was calibrated with weights.

Results (TTT)

All specimens failed in the composite rather than at the adhesive bond. Some failures occurred so close to the ends that the failure plane cut through the adhesive fillet and these were not considered good tests. Failure planes in the B material were randomly located. Those of the A materials were predominantly at one end. The locations of each failure are marked in Figure 28. Although some failures occurred close (within one fabric layer) to the special material planes, none actually caused separation of those planes.

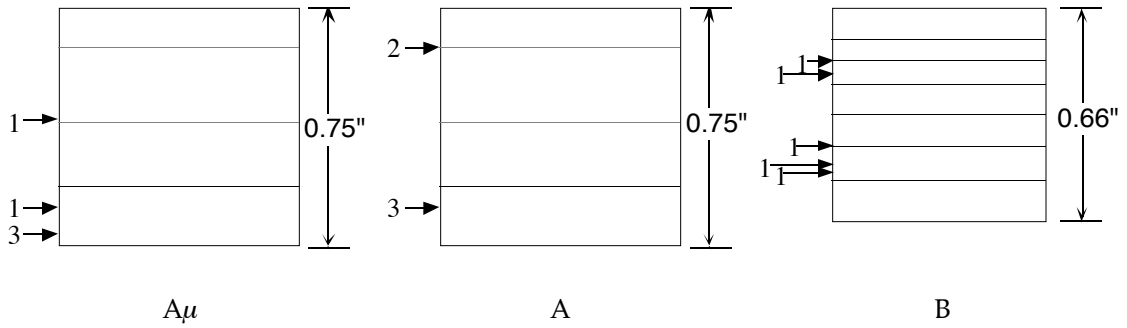

Figure 28. Through-thickness tensile failure locations. Arrows denote location and number of failures.

A summary of the tensile strengths is given in Table 14. These low values are not surprising considering the transverse in-plane tensile strength of unidirectional material is only 1 ksi (Table 4). Both the irregular surfaces between fabric layers and the presence of microspheres probably cause a reduction in the through-thickness strength below this value.

Table 14. Through-thickness tensile strength data.

Material	Specimen	Through-Thickness Tensile Strength (psi)
Aμ	1	288
Aμ	3	314
Aμ	4	277
Aμ	6	307
Aμ	7	341
Aμ	Average (SD)	**306** (24.7)
A	1	728
A	2	768
A	3	688
A	4	591
A	5	594
A	Average (SD)	**677** (79.4)
B	2	564
B	3	560
B	4	564
B	5	592
B	6	564
B	Average (SD)	**569** (13.0)

3.6 In-Plane Shear (IPS)

Experimental (IPS)

To measure the in-plane (and out-of-plane or interlaminar) shear stress-strain behavior, we chose to use the V-notch beam shear specimen which was first proposed by Iosipescu [5] and has become an ASTM standard [6]. We originally elected to use the Asymmetric Four-Point Bend (AFPB) loading scheme for this specimen, as our previous work with the AFPB test applied to thick carbon/epoxy and aluminum materials was quite successful. In our opinion, the AFPB scheme applies load in a more defined and uniform way than in the Iosipescu method, though others consider this debateable [7,8]. The Iosipescu loading is a displacement-controlled scheme where the distribution of loads on the surface of the specimen are not well-defined. Numerical modeling has shown that the shear stress distribution between the notches of a 0° specimen is sensitive to location of the applied loads [9]. The advantage of this method is that it prevents bending if the fixture is relatively stout.

Our first attempts using the AFPB method were unsuccessful because the material suffered bending failure instead of shear. While these problems can be corrected by moving the major load points further out from the specimen centerline, all specimens had already been machined to length and we were already at the maximum separation. By making some simple modifications to our test fixture, we converted it to an Iosipescu-like fixture having more clearly defined load points than the popular Wyoming test fixture. A schematic of the fixture used for all our V-notch beam shear tests is shown in Figure 29. The clamping arrangement for this fixture precisely defines the load points at the major span. Also, the precision guide bars keep the two loading surfaces parallel during loading.

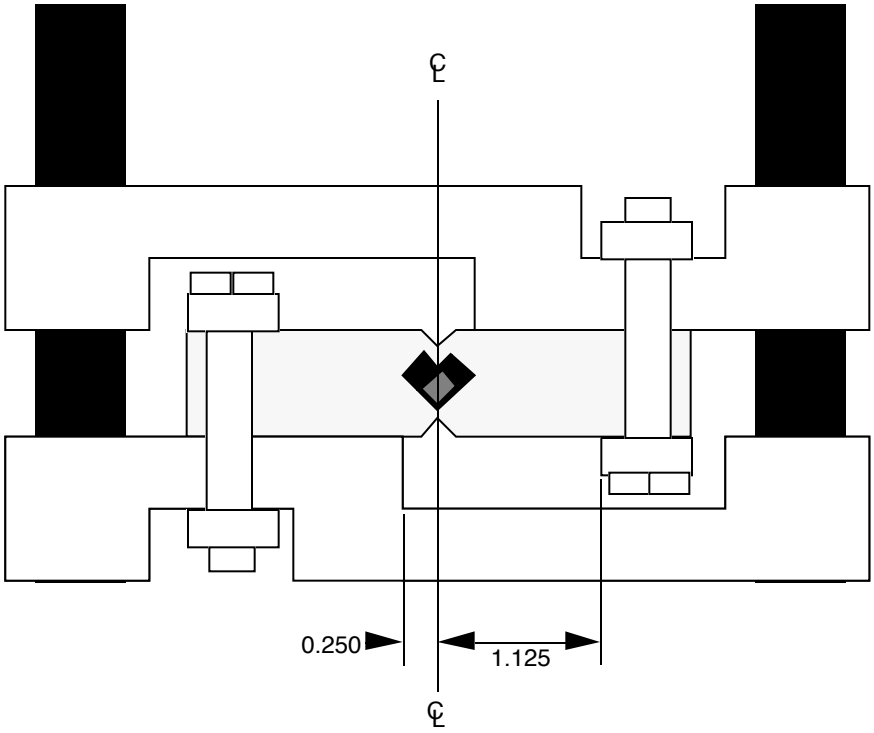

Figure 29. V-notch beam shear test fixture.

The following description of the shear tests also applies to the out-of-plane or interlaminar shear tests described later. We followed the ASTM standard D5379 as closely as possible for these tests. Our final specimen geometry is based on the recommendations in this procedure and is shown schematically in Figure 30. Shear strains were measured using stacked biaxial gages (Measurements Group-CEA-13-125WT-350) on both surfaces of the beam. The strain was calculated by averaging the values from the two sides. Tests were performed at a nominal stroke rate of 0.050 in/min on a model 1125 Instron equipped with an electronically calibrated 2 kip load cell. The validity of the test set-up was determined by testing for the shear properties of T6061-T651 aluminum having the same specimen geometry as the sonar materials, except these were only 0.375" thick to allow failure loads to be somewhat closer to those expected for the composite materials.

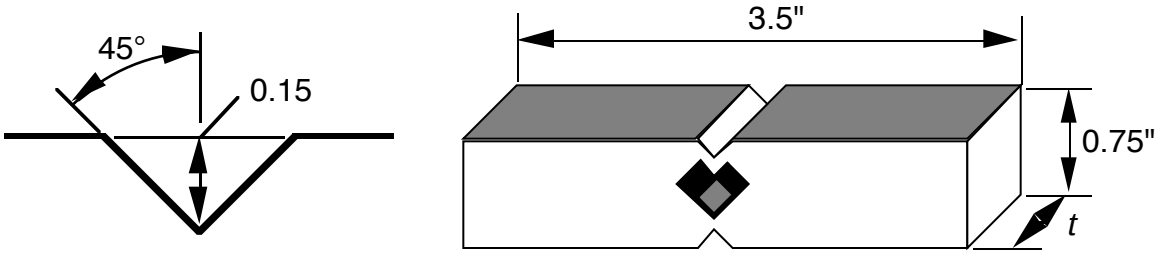

Figure 30. In-plane V-notch beam shear test specimen.

Results (IPS)

Aluminum Calibration Specimen: A typical shear stress-strain curve for an aluminum specimen is shown in Figure 31. An average shear modulus of 3.69 ± 0.21 Msi and shear strength of 35.6 ± 1.2 ksi was measured from three specimens. The modulus is close to the handbook value of 3.75 Msi, but this strength, which is the maximum and not the fracture stress, is somewhat higher than the handbook value of 30 ksi [4]. Failure surfaces were clean breaks between the notches, but oriented slightly off the vertical. Failure strains were on the order of 20%.

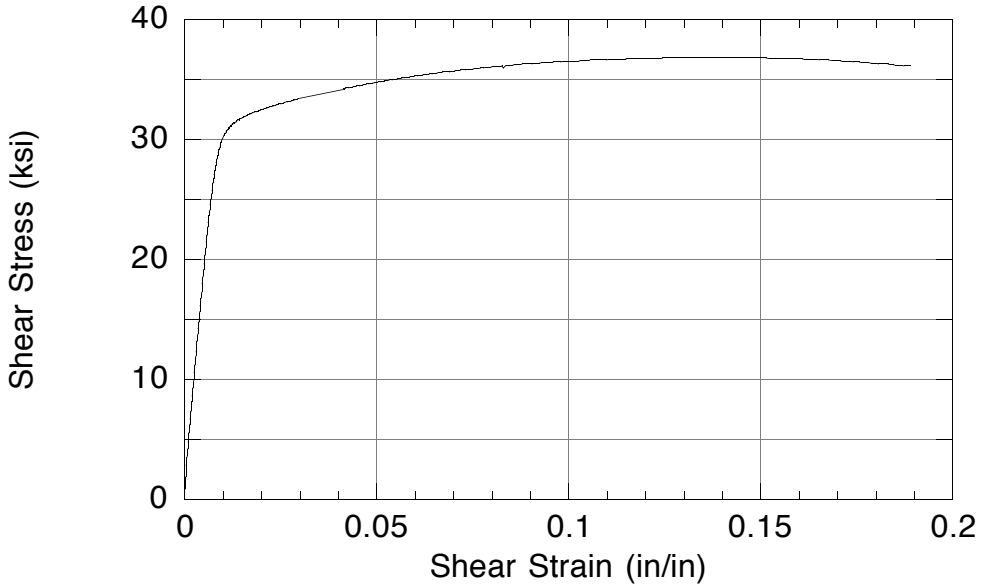

Figure 31. Shear behavior of 6061-T651 aluminum.

Constitutive Behavior: The sonar materials all exhibited nonlinear behavior and curves for three samples of each material are shown in Figures 32-34. There was significant variation among the B specimens, but both the A materials exhibited reproducible response. No clear failure point was ever attained and in most cases the testing was halted because the fixture bottomed out. Although shear strains greater than 5% were measured for all specimens, values greater than this are suspect because the samples started to fail in compression near the notches. This failure was noticed by the lateral bulging of the material at its centerline, which would disturb the strain gage readings. After testing, all specimens retained a permanent set corresponding to a significant percentage of the total applied shear strain. In the A specimens, some delamination occurred at the darkest special material plane. In fact, this plane is much stiffer and stronger than the composite and recovered much more of the shear strain than the Spectra composite.

Linear fits to the small strain regions of the curves yielded the shear moduli listed in Table 15. The nonlinear behavior was fit to data up to approximately 3% strain using the Ramberg-Osgood relationship. The average fits to all the specimens of each type are plotted in Figure 35 and the parameters given in Table 16. This comparison shows the higher rigidity of the A composite.

Table 15. In-plane shear moduli.

Material	Specimen	G_{12} (ksi)
Aμ	2	160
Aμ	3	130
Aμ	4	140
Aμ	Average (SD)	**144** (15.2)
A	1	230
A	3	220
A	4	220
A	Average (SD)	**223** (5.7)
B	2	61
B	4	130
B	Average (SD)	**100** (49)

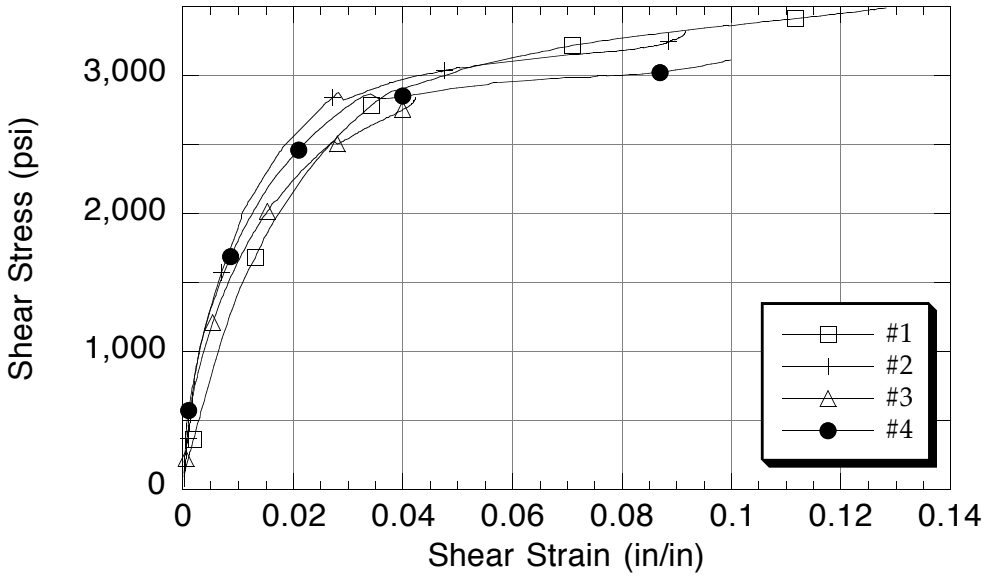

Figure 32. In-plane shear behavior of Aμ specimens.

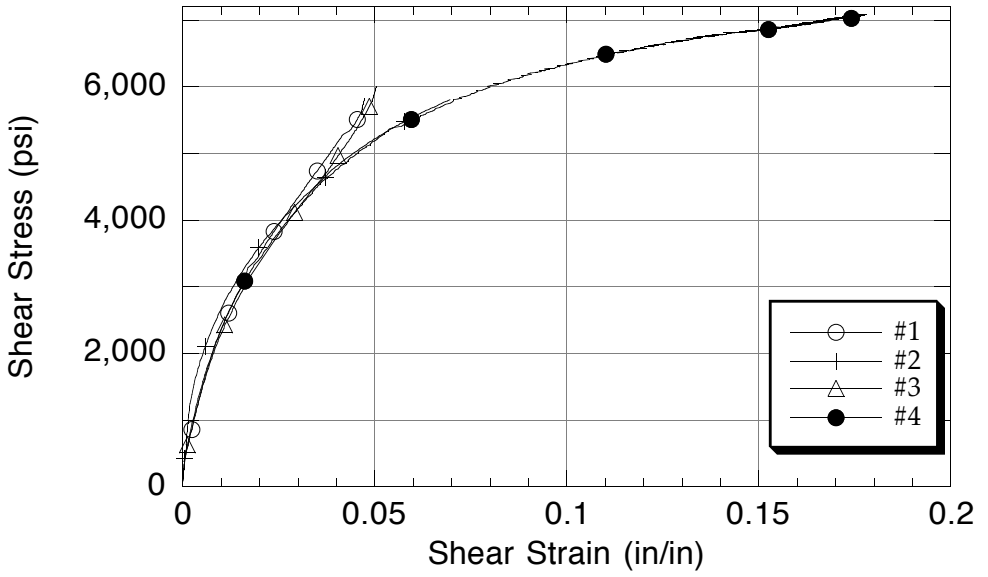

Figure 33. In-plane shear behavior of A specimens.

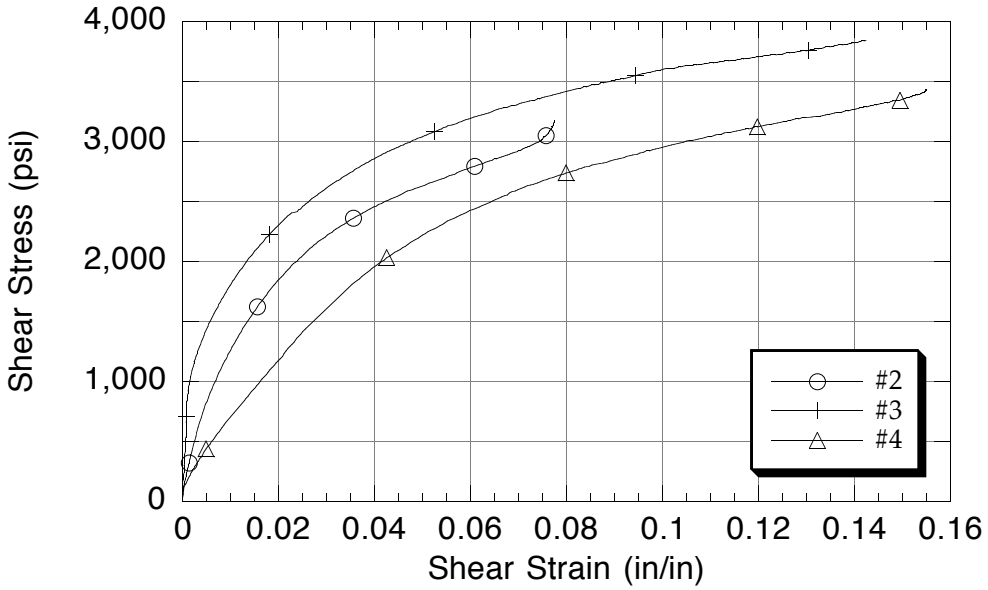

Figure 34. In-plane shear behavior of B specimens.

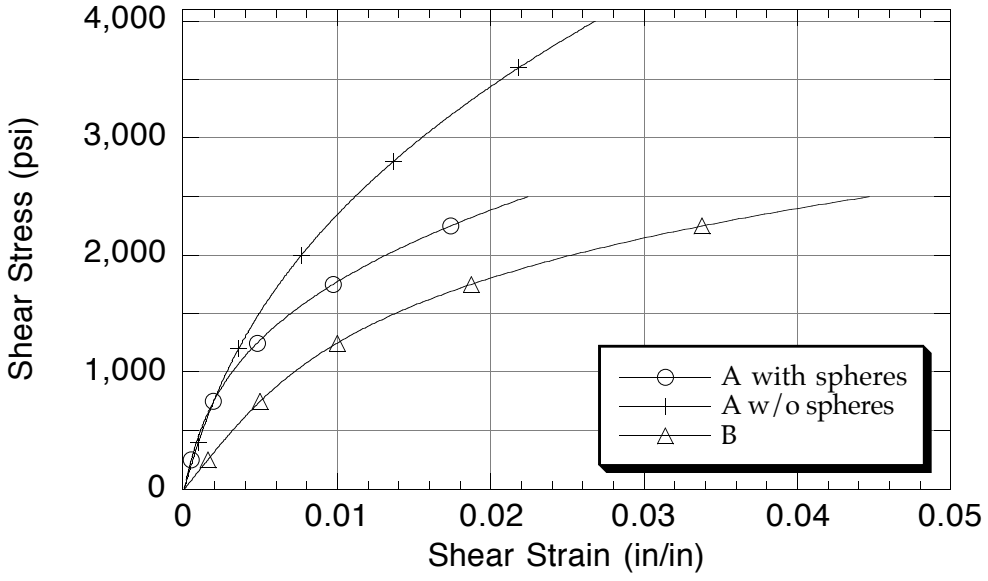

Figure 35. Average Ramberg-Osgood fits to in-plane shear behavior.

Table 16. Ramberg-Osgood fit parameters for in-plane shear.

Material	G_{12} (ksi)	σ_o (ksi)	β
Aμ	**580** (139)	1.12 (0.28)	2.8 (0.20)
A	**461** (23)	2.4 (0.17)	2.5 (0.06)
B	**163** (40)	2.0 (0.38)	3.6 (0.77)

3.7 Interlaminar Shear (ILS)

Results (ILS)

Constitutive Behavior: The out-of-plane or interlaminar shear stress-strain behavior was measured using the same procedure as for the in-plane shear tests. Results for the three materials are plotted in Figures 36-38 and the Ramberg-Osgood fits to the average curves for the A and the B composites are shown in Figure 39. Linear fits were made to the small strain regimes to determine the initial shear moduli given in Table 17. Because of the large variation in the results, no attempt was made to fit a nonlinear curve to the Aμresponse. The parameters for the nonlinear fits to the average curves of the other two composites are listed in Table 18.

Table 17. Interlaminar shear moduli.

Material	Specimen	$G_{13} = G_{23}$ (ksi)
Aμ	2	44
Aμ	3	43
Aμ	Average (SD)	**44** (0.7)
A	1	170
A	2	190
A	3	170
A	Average (SD)	**177** (11.5)
B	1	80
B	2	130
B	3	100
B	Average (SD)	**103** (25)

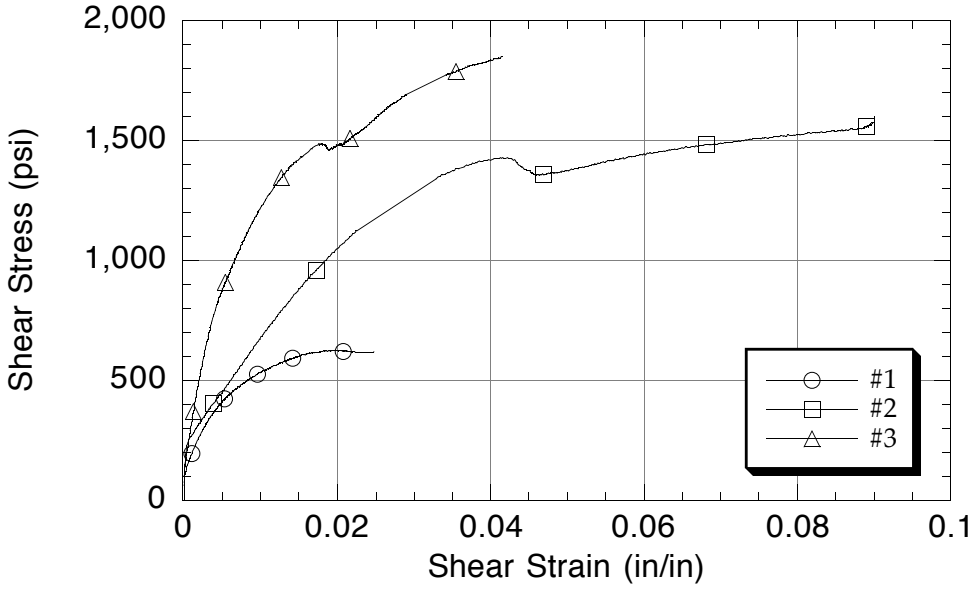

Figure 36. Interlaminar shear behavior of Aμ specimens.

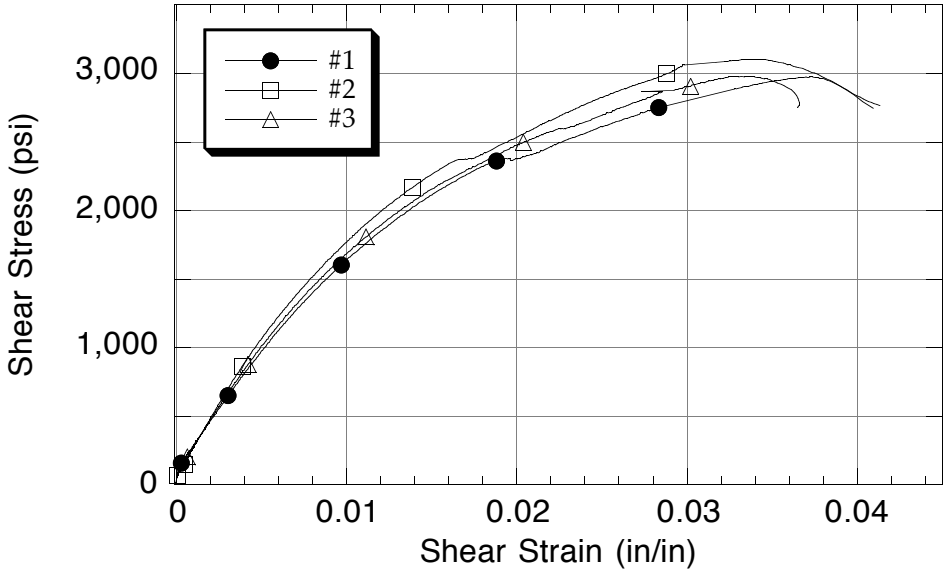

Figure 37. Interlaminar shear behavior of A specimens.

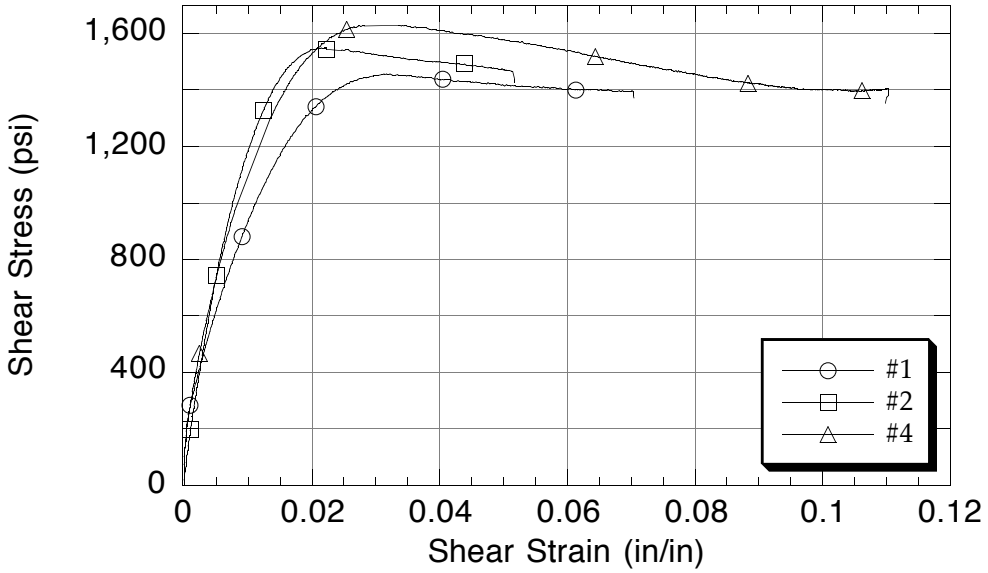

Figure 38. In-plane shear behavior of B specimens.

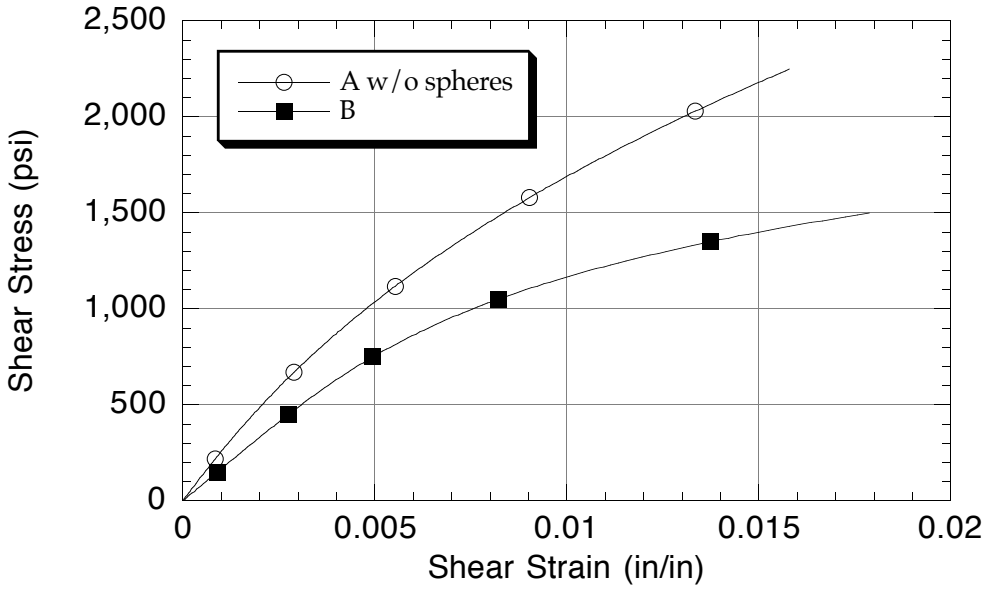

Figure 39. Average Ramberg-Osgood fits to interlaminar shear behavior.

Table 18. Ramberg-Osgood fit parameters for interlaminar shear.

Material	$G_{13} = G_{23}$ (ksi)	σ_0 (ksi)	β
A	**267** (5.2)	5.2 (0.06)	2.4 (0.06)
B	**167** (2.7)	1.5 (0.01)	4.3 (0.13)

Failure: All tests were run until the fixture reached its maximum travel. The only indication of a shear failure plane in any of the specimens was cracking at the notch roots in the Aμmaterial. Neither of the other two composites showed any signs of visible cracks. Ideally, the strengths measured in these tests could be compared with those determined using the notched interlaminar shear (NILS) strength test. For all the V-notch interlaminar tests, the maximum shear stresses, which are given in Table 19, were higher than the corresponding strengths obtained from the NILS tests. The ability to determine shear failure in V-notch beam specimens having fibers aligned along the beam axis is also a subject of debate. Typical observations for 0˚ carbon/epoxy specimens are the formation of cracks at the root of the notch followed by a stress increase to a point where shear cracks form between the notches. For the A specimens, there is a small plateau in the curves at around 2.5 ksi (Figure 37) and this stress is identical to the strength measured in the NILS tests. For the other specimens, no obvious features were seen in the stress-strain curve at the stress levels corresponding to failure in the NILS tests. The unloaded specimens recovered nearly 100% of the applied shear deformation. If the interlaminar shear behavior is dominated by the matrix properties, recovery of the relatively large strains applied during these tests would not be expected. The full recovery observed might imply that fiber deformation occurred during these tests. If so, then the maximum stress values would not be indicative of true interlaminar shear failure.

Table 19. Maximum shear stress from V-notch interlaminar shear tests.

Material	Specimen	Maximum Shear Stress (ksi)
Aμ	1	0.64
Aμ	2	1.64
Aμ	3	1.85
Aμ	Average (SD)	
A	1	2.97
A	2	3.10
A	3	2.98
A	Average (SD)	**3.02** (0.07)
B	1	1.46
B	2	1.55
B	4	1.63
B	Average (SD)	**1.55** (0.09)

Discussion

The following discussion will refer to the primary goals of this work which were outlined in the introduction to this report (pg. 7).

1. Elastic Constants: The elastic constants are summarized in Table 1, pg. 2. The values, especially those for material A, are reasonable considering the reported elastic constants for the unidirectional material (Table 4, pg. 6).

For the IPT and TTC tests, cycling the load revealed that the materials undergo strain-hardening after the first cycle, although the IPT tests are complicated by grip effects. In both tests, the response became somewhat reproducible after three cycles in the same stress range. Although the other properties were measured from single loading tests, it is expected that these constants can also change with cycling.

The modulus E_{11} and Poisson's ratios ν_{12} and ν_{13} were measured in both tension and compression. For analysis, it is recommended that the values obtained from the compression tests be used. The IPT test data are less reliable because relatively high stresses (>2 ksi) were required to seat the specimen in the grips and therefore the small-strain behavior is masked. Additionally, there is a satisfactory agreement in that the in-plane modulus measured in compression is about half the tensile modulus of the unidirectional material. The reported compression modulus of the unidirectional material is unusually low, which may be due to the problems defining an initial modulus for the highly nonlinear response in compression. In tests performed in this study, effort was made to obtain data at strains less than the fiber failure strain in compression (ca. 0.1%). Consequently, the initial moduli measured from these tests are in much better agreement with the tensile moduli. Cycling to strain levels above the fiber failure point is expected to generate damage and alter the stress-strain response.

For the material symmetry assumed where 1- and 2-directions are equivalent, there are six unique elastic constants. The seven property values in Table 1 have a redundancy which can be checked using the identity relationship

$$\frac{\nu_{13}}{E_{11}} = \frac{\nu_{31}}{E_{33}}$$

Using the values of E_{11} and ν_{13} measured in compression and comparing with the values of E_{33} and ν_{31} reveals that this identity is only satisfied for the B composite. Of the four properties needed for this relationship, the Poisson's ratio ν_{31} is the most uncertain due to the error in measuring small lateral strains.

Therefore, it is recommended that this value be adjusted to satisfy the identity. The adjusted values are 0.026 for A and 0.015 for Aμ.

The moduli E_{33} measured for A and Aμ in compression are similar to the reported transverse modulus of the unidirectional material. The corresponding value for material B is significantly higher. This value is very sensitive to both the matrix properties and fiber content and it may be that the B material has a higher modulus epoxy and/or a different fiber content than the A materials.

Both the in-plane and interlaminar shear moduli of all three materials fell within the range of 0.044–0.22 Msi, which compares favorably with the unidirectional in-plane shear modulus of 0.12 Msi.

2. Stress-Strain and Failure: All the response curves for the three materials were nonlinear to different degrees. Cycling the TTC and IPT specimens revealed that strain-hardening occurred during the first cycle, but that more repeatable behavior could be obtained after three cycles. In both cases there was hysteresis, but little permanent set. The apparent plastic deformation in the IPT tests (Figure 23) is most likely due to grip effects.

While nonlinear fits such as the Ramberg-Osgood relationship could be used to model the behavior in all load cases, some simplifying assumptions could be made without much loss in accuracy.

After some initial cycling, the IPT behavior could be adequately described with a linear fit, at least up to stress levels of about 20 ksi. The TTT tension response, although not measured, is most likely linear up to the small failure strains (ca. 0.3%). This response could be modeled using the modulus and Poisson's ratio measured in TTC.

The nonlinear Ramberg-Osgood fit was applied to the IPC curves and the parameters for moduli and Poisson's ratios up to 0.4% compression strain are given in Tables 8-10. However, the shapes of the stress-strain and lateral strain-longitudinal strain curves suggest that a reasonable approximation to the data could be made using a bilinear fit up to the failure stress.

The TTC behavior is roughly linear in loading after the materials have been cycled a few times. There is significant strain-hardening during the first cycle, but the behavior in subsequent cycles is repeatable and nearly linear on loading. More accurate representation of both the loading and unloading curves could be made with polynomial fits.

Both the IPS and OPS response are highly nonlinear and it is recommended that nonlinear fits such as the Ramberg-Osgood relationship used in this study be

used to model these properties. Very rough approximations could be made using bilinear curves if the capability to use nonlinear material models isn't available.

Failure was not achieved in the IPT, IPS, and the TTC tests and only lower bound values for strength are tabulated in the Abstract (pg. 3). The relatively high stress bounds in IPT (>50 ksi) and TTC (>100 ksi) should be more than adequate for modeling sonar windows. It is highly unlikely that stresses approaching these levels will ever be achieved in practice before some other failure mode sets in. Likewise, the IPS specimens were taken to strains greater than 10% without a shear failure occurring and it is improbable that such strains would be achieved in application. In fact, these tests were limited by the onset of in-plane compression failure, which demonstrates the tendency for these materials to fail in weaker modes.

The IPC compression strengths ranged from 4.1 to 8.0 ksi and these values compare well with the reported 10.5 ksi 0˚ compression strength of unidirectional Spectra 1000/epoxy composite. Because of the relatively poor fiber compression strength, the IPC is strongly dependent on the matrix and fiber/matrix bond strengths. Any differences in compression strength are probably attributable to the disparities in the matrix and interface strengths.

The interlaminar shear strengths were measured using both the notched compression and the V-notch beam specimens. There is some controversy regarding the best method for determining interlaminar shear strengths and for this reason two separate tests were conducted to at least define a range of values. The more popular short-beam interlaminar shear strength test was not considered since the material is weak in compression and the properties of the special material planes, which are needed to determine the shear stress in bending, are unknown. The notched compression test yielded clearly defined maximum loads and fracture planes. In contrast, the V-notch beam specimens yielded definite maximum stress values for A and B materials, but not the Aμ composite. Also, the only fracture planes observed were cracks at the notch roots in the Aμ specimens. The strengths of the A and B composites determined using the V-notch specimens were 21% and 65% greater than the corresponding notched compression test values. The V-notch beam interlaminar shear strength could not be determined for the Aμ composite because there was no clear failure point.

It is recommended that the values obtained from the notched compression tests be used for analysis for the following reasons. (1) It was the only test where a clearly defined shear failure occurred. (2) The interlaminar shear strength of a unidirectional composite is only 1.7 ksi and of a 951 PT fabric composite is 2.2 ksi, which are in the range of strengths measured in the notched compression test. (3) Use of these values in a stress analysis of the sonar windows would be conservative.

3. Special Material Planes: All failures where clearly defined fracture surfaces were observed occurred at locations away from the special material planes. This indicates that the properties measured here are primarily for the Spectra/epoxy composites and that the removal of these planes would have little effect on the mechanical performance of the materials. There may have been some local stress effects in the A and Aμmaterials near the darkest layer. This layer is obviously stiffer and stronger than the Spectra composite and the mismatch in properties may have led to edge stress singularities in certain tests such as the TTT. Without knowing the properties of these special layers it is hard to determine the contribution of the edge stresses to failure.

4. Accuracy of Tests: The 6061-T651 aluminum calibration specimens used in the IPC, NILS, and V-notch beam tests yielded values of moduli and strengths which were in excellent agreement with handbook values. The only exception was the shear strength measured using the V-notch beam test. There is no description in the handbook reference on the technique used to measure shear strength and the ASTM standards for shear testing of aluminum doesn't include the V-notch beam specimen. The close agreement between the strength measured in this study using the notched compression specimen (31.8 ksi) and the handbook value (30 ksi) suggests that a similar test was used to generate the book value. While the Iosipescu test of the V-notch beam specimen was originally proposed as an accurate method for determining shear strength of metals, it is unclear if the stress state between the notches remains pure up to shear strains of 20%. In all of the specimens tested, the failure plane was oriented away from the vertical by about 5˚ and the root of the notch showed signs of distortion due to compression. Other tests (e.g., shear strength measured using torsion tubes) need to be conducted to determine which method yields accurate shear strengths.

Conclusions

The data presented in this report for the three-dimensional mechanical behavior of Spectra/epoxy sonar window materials show that many of the properties of these composites are inferior to a pure epoxy. The exceptions to this are the fiber-tension dominated properties — the IPT stiffness and strength — and the TTC strength. In general, it can be concluded that these composites are not robust structural materials.

The few tests in which the effects of cycling were examined revealed that the materials exhibit permanent changes after loading to small stress levels. The changes are presumably due to some damage which could affect acoustic performance. Although we did not examine the effects of cycling on the IPC behavior, the fiber kinking which occurs at low compression strain levels is a form of damage that could also interfere with acoustic transparency and the long-term mechanical performance under fatigue loads.

Acknowledgment

The authors wish to acknowledge the support of Mike Thiry for water-jet machining, Will Andrade for sample preparation and machining, Dennis Freeman for testing and Janet Conrad for help in editing this report. We also appreciate the encouragement of Dr. Y. D. S. Rajapakse of the Office of Naval Research.

References

1. **Spectra High Performance Fibers for Reinforced Composites,** Allied-Signal Inc., High Performance Fibers, Petersburg, VA.

2. H. X. Nguyen, Allied-Signal Inc., Private communication (1988).

3. S. J. DeTeresa, S. R. Allen and R. J. Farris in **Composite Applications: The Role of Matrix, Fiber, and Interface**, T. Vigo and B. Kinzig, eds., VCH, New York, 1992, pp. 67–106.

4. **Metals Handbook, 10th Edition, Vol. 2, Properties and Selection: Nonferrous Alloys and Special-Purpose Materials**, ASM International, 1990, pg. 102.

5. N. Iosipescu, "New Accurate Procedure for Single Shear Testing of Metals," *J. Mater.* **2**(3) 537 (1967).

6. ASTM D 55379/ D 5379M - 93, "Standard Test Method for Shear Properties of Composite Materials by the V-Notched Beam Method," Annual Book of ASTM Standards, Vol. 15.03, pp 235–247 (1995).

7. M. G. Abdallah and H. E. Gascoigne, "The Influence of Test Fixture Design of the Iosipescu Shear Test for Fiber Composite Materials," **Test methods and Design Allowables for Fibrous Composites: 2nd Volume, STP 1003**, C. C. Chamis, Ed., ASTM, Philadelphia, 1989, pp. 231-260.

8. D. F. Adams and D. E. Walrath, "Current Status of the Iosipescu Shear Test Method," *J. Comp. Mater.*, **21**, 494 (1987).

9. J. Morton, H. Ho, M. Y. Tsai and G. L. Farley, "An Evaluation of the Iosipescu Specimen for Composite Materials Shear Property Measurement," *J. Comp. Mater.*, **26**(5) 708 (1992).

Technical Information Department • **Lawrence Livermore National Laboratory**
University of California • Livermore, California 94551